DEVELOPMENT OF A CANDLE FILTER FAILURE SAFEGUARD DEVICE

FINAL REPORT

Contract No. DE-AC26-99FT40678

Principal Investigator: Todd R. Snyder

Southern Research Institute

March 29, 2002

Project Manager: Ted McMahon

for

UNITED STATES DEPARTMENT OF ENERGY
National Energy Technology Laboratory
Post Office Box 880, 3610 Collins Ferry Road
Morgantown, West Virginia 26505

ABSTRACT

The full-flow mechanical safeguard device (FFMSGD) has been developed under contract to the National Energy Technology Laboratory (NETL) to address problems with the reliability of ceramic candle filter elements installed on high-temperature, high-pressure (HTHP) Hot Gas Cleanup (HGCU) filters. Although systems candle filters are expected to perform satisfactorily when in good operating condition, the failure of even a single filter element can increase the filter system outlet dust loading enough to potentially damage gas turbine blades, contaminate other downstream processes, and limit the availability of the power system. Filter failure safeguard devices that are installed on each individual candle filter element are envisioned as a guarantee of a candle filter system's ability to withstand some number of element failures and continue operation without these negative consequences. The intention of the FFMSGD is to provide this guarantee without incurring any significant pressure drop penalty or constraining the filter system's reverse-pulse cleaning procedures. The FFMSGD provides a clear flow path for filtered and reverse-flow cleaning gases when its filter element is intact, and activates to provide a positive mechanical seal against gas flow in either direction when its filter element breaks or fails. This activation is induced by the increase in the flow rate of gas through the device in event of filter failure. The FFMSGD is designed to be easily removed and reconditioned when the filter system is taken off line for routine maintenance.

This report is intended to be issued with a companion appendix. As instructed in Section J.12 of Contract No. DE-AC26-99FT40678, all the restricted, proprietary, and patentable information (not yet disclosed through the patent application process) related to the FFMSGD and its evaluation under this contract has been included only in the appendix. This Final Report, which is available to the public, contains background information and general descriptions of the operating principles of the FFMSGD. This report also describes the results of various evaluations of the device at room temperature and in HTHP environments. This Final Report also includes discussions of commercialization issues. For clarity and completeness, all of the information contained in this Final Report has also been included in the appendix.

TABLE OF CONTENTS

PAGE

LIST OF TABLES

LIST OF FIGURES

EXECUTIVE SUMMARY

Under Task 1 of this contract, an initial prototype (P1) was designed, fabricated, and tested at ambient conditions. The results of Task 1 were reported in a topical report and companion appendix. A test plan for high-temperature tests was prepared under Task 2. Under Task 3 a second prototype FFMSGD (P2) was designed for high-temperature testing and subsequently fabricated under Task 4. The evaluation of P2 was conducted under Task 5. Project activities continued under Options I and II of this contract, which have culminated in the design, fabrication, and testing of a third prototype (P3). Ambient-condition testing of P3 has been followed by a limited high-temperature evaluation of P3 at the Department of Energy / Southern Company Services Power Systems Development Facility (PSDF).

This report summarizing all project activities was prepared along with its companion appendix. As instructed in Section J.12 of Contract No. DE-AC26-99FT40678, all the restricted and patentable information (not yet disclosed through the patent application process) related to the FFMSGD and its evaluation under this contract have been included only in the appendix, which is available for review by DOE personnel only. For clarity, all of the information contained in this Final Report has also been included in the appendix. This Final Report, which is available to the public, discusses the objectives, and the majority of the test procedures and results of the various evaluations of the FFMSGD concept. These evaluations included characterizations of the performance of three generations of FFMSGD prototypes (P1, P2, and P3) at ambient conditions at Southern Research Institute's laboratory in Birmingham, Alabama. The evaluations also included extensive tests (at ambient temperature and HTHP conditions - about 1500 °F and 70 psig) of P2 conducted in the Small Pressure Vessel (SPV) at DOE/NETL's High-Temperature Gas-Stream Cleanup Test Facility (HTGSCTF) during June and July 2000. The third prototype, P3, is currently installed at the PSDF for evaluation in a HTHP gasification test run.

The proof-of concept prototype, P1, proved very successful in the Task 1 ambient temperature tests, activating quickly and reliably with and without the presence of entrained ash. The seal it formed remained intact in the presence of strong reverse-gas pulses. The high-temperature prototype FFMSGD, P2, performed very well in the tests in Task 5. Activation of the device was repeatedly achieved at ambient and HTHP conditions. The FFMSGD activated quickly and completely, and remained activated (closed) when exposed to vigorous reverse-gas cleaning pulses. The FFMSGD also withstood these vigorous reverse-gas cleaning pulses in its inactive (open) mode with no apparent effect. The threshold of activation for the FFMSGD is properly quantified in terms of the quantity ρv^2, where ρ is the density of the gas passing through the FFMSGD, and v is the velocity of the gas through the minimum annular orifice in the device. The threshold of activation for P2 was consistent for almost all the test runs performed at both ambient and HTHP conditions. To the extent provided by the PCME device used to measure outlet mass levels at the HTGSCTF, the activation of P2 quickly and consistently formed a high-quality seal. Post-test visual inspection of the seal formed by the FFMSGD when it activated at ambient and HTHP conditions suggests that the device formed a total barrier to the passage of particles, and also to the flow of gas. In addition, P2 offered very little resistance to the flow of filtered gas (ΔP across P2 was less than 1.5 in. H_2O at a flow of 30 acfm) prior to its activation.

Although the test designed to assess the effect the presence of the FFMSGD had on cleaning effectiveness had to be aborted due to filter element failure, there is every reason to believe that the low resistance to flow in the forward (normal) direction translates to an equally low interference with the effectiveness of reverse-gas cleaning pulses.

The pilot-scale evaluations of P3, which are ongoing at the time of the preparation of this Final Report, are principally designed to determine if P3 will remain inactive (open) during normal HTHP operation of the PSDF, and if it can be successfully activated after extended exposure to HTHP conditions. Because the evaluations of P3 at the PSDF are ongoing, the final results of these evaluations cannot be included in this Final Report or its companion appendix. However, the results of the evaluations of P3 at the PSDF that are available at this time are included here.

SGD PERFORMANCE CRITERIA

Over the past decade, a variety of filter designs based on porous ceramic filter elements have been developed to provide cleanup of particulate-laden flue gas at high temperatures and high pressures. The most common filter design has been based on multiple rigid, cylindrical ceramic filter tubes placed in parallel across the process stream. The process conditions to which these filter designs have been exposed have taxed the capabilities of the ceramic materials used to construct the individual filter elements, resulting in periodic failures of a significant proportion of these filter elements. Because the components downstream of these HTHP filters can be extremely sensitive to even small amounts of entrained particulate matter, these failures have revealed the need for a means to ensure the cleanliness of the flue gas downstream of the filter in the case of catastrophic failure of some portion of the filter components. Consequently, the requirements of any system or safeguard device designed to deal with these failures must be quite stringent.

In 1999, the Department of Energy's National Energy Technology Laboratory (DOE/NETL) issued a competitive solicitation (RFP No. DE-RP26-99FT40199) to develop suitable SGD's for inclusion in Hot Gas Cleanup (HGCU) systems envisioned for advanced PFBC and IGCC facilities. The criteria for a successful SGD design require that:

- the SGD must be able to operate with either PFBC ash or IGCC char with flue gases that may be either oxidizing (PFBC) or reducing (IGCC);
- in the event of the catastrophic failure of its filter element, the SGD must activate quickly and reliably, and once activated, provide a continuous barrier to prevent particles that breach its failed filter element from crossing the tubesheet;

- the SGD should have zero particulate emissions when in its active mode of operation, although low (~ 1-2 ppm) and or periodic emissions could conceivably be tolerated;
- at the time of filter failure, the SGD must be able to function with a dust loading of 2,000 to 20,000 ppm (or higher);
- the SGD must endure long-term operation at operating temperatures from 700 to 1600° F;
- the SGD must endure long-term operating pressures from 150 to 400 psia;
- the SGD design must be able to treat a nominal gas flow of 10 - 100 acfm when its filter is intact and the SGD is in its inactive mode of operation (in order to cover a wide variety of candle filter lengths and candle filter face velocities);
- the SGD must be able to activate with a nominal gas flow through it of 20 to 200 acfm when a filter fails and SGD operation is initiated;
- the SGD must withstand repeated, vigorous, back-pulse cleaning events in its inactive and active operational modes;
- in its inactive mode, the SGD must not impede effective reverse-pulse cleaning of its intact filter element;
- the candidate SGD must be able to remain in either its inactive or activated condition throughout the variety of operating conditions liable to be encountered during normal HGCU filter operation (system startups and shutdowns, load changes, and variable temperatures and face velocities, etc.);
- the flow resistance of the SGD when in its inactive mode of operation (with an intact filter element) should be minimized; and
- the SGD design must be able to integrate into existing filter system designs in terms of seals, gaskets, fixtures, and assemblies.

In addition to these technical constraints, the most desirable SGD design should be inexpensive, easy to install, and easy to restore to its inactive mode during off-line servicing of the HGCU filter assembly.

Southern Research Institute (SRI) used its extensive experience with a wide variety of technologies associated with the capture of entrained particulate matter from flue gas streams to propose a unique SGD design in response to DOE/NETL's solicitation. In order for an SGD to meet the criteria listed above, it must be able remain inactive, and then to activate only in response to the conditions it experiences immediately following the failure of the filter element it is designed to service. When a filter element undergoes catastrophic failure, two primary events occur. Because the breach of the ceramic filter element (and its associated filter cake, if any) provides a localized, much lower resistance flow path across the filter assembly's tubesheet, gas flow through the inactive SGD immediately increases greatly following a filter element failure. In addition to this change, dust-laden gas enters the portion of the filter element remaining on the tubesheet. Without the advantage of additional sensors to detect and identify the failure of a particular filter element, one or both of these two events must be able to trigger the activation of the SGD. It is possible to envision static SGD designs that act as a secondary filter, or particle trap, in the event of filter element failure. However, because reliably capturing and retaining particles in an SGD requires suitably small

pores, the passage of clean gas in the inactive mode would lead to an unacceptable pressure drop penalty, as well as potentially interfering with effective reverse-pulse cleaning. There is also the possibility that an SGD that functions as a particle trap might be susceptible to reentraining previously captured particles when exposed to the force of periodic reverse-gas pulses. Based on these factors, the design of SRI's SGD (discussed in detail below) makes use of the increase in gas velocity through the SGD associated with a filter element failure to trigger SGD activation. Once this approach was selected, the challenge was to generate a design for a mechanical check valve that would function reliably and predictably at the extremely harsh conditions found in HGCU filters.

The FFMSGD concept described below is designed to meet all the objectives established by DOE. The data and observations presented in this report demonstrate that the various prototype FFMSGDs designed, constructed, and tested in this project met all the performance criteria that were possible to measure given the various HTHP systems available for testing. (Tests that would be required to meet the few criteria that could not be evaluated during this project are discussed at the end of this report.)

THEORY OF FFMSGD OPERATION AND GENERAL DESIGN FEATURES

The basic concept of the FFMSGD is shown in Figure 1.

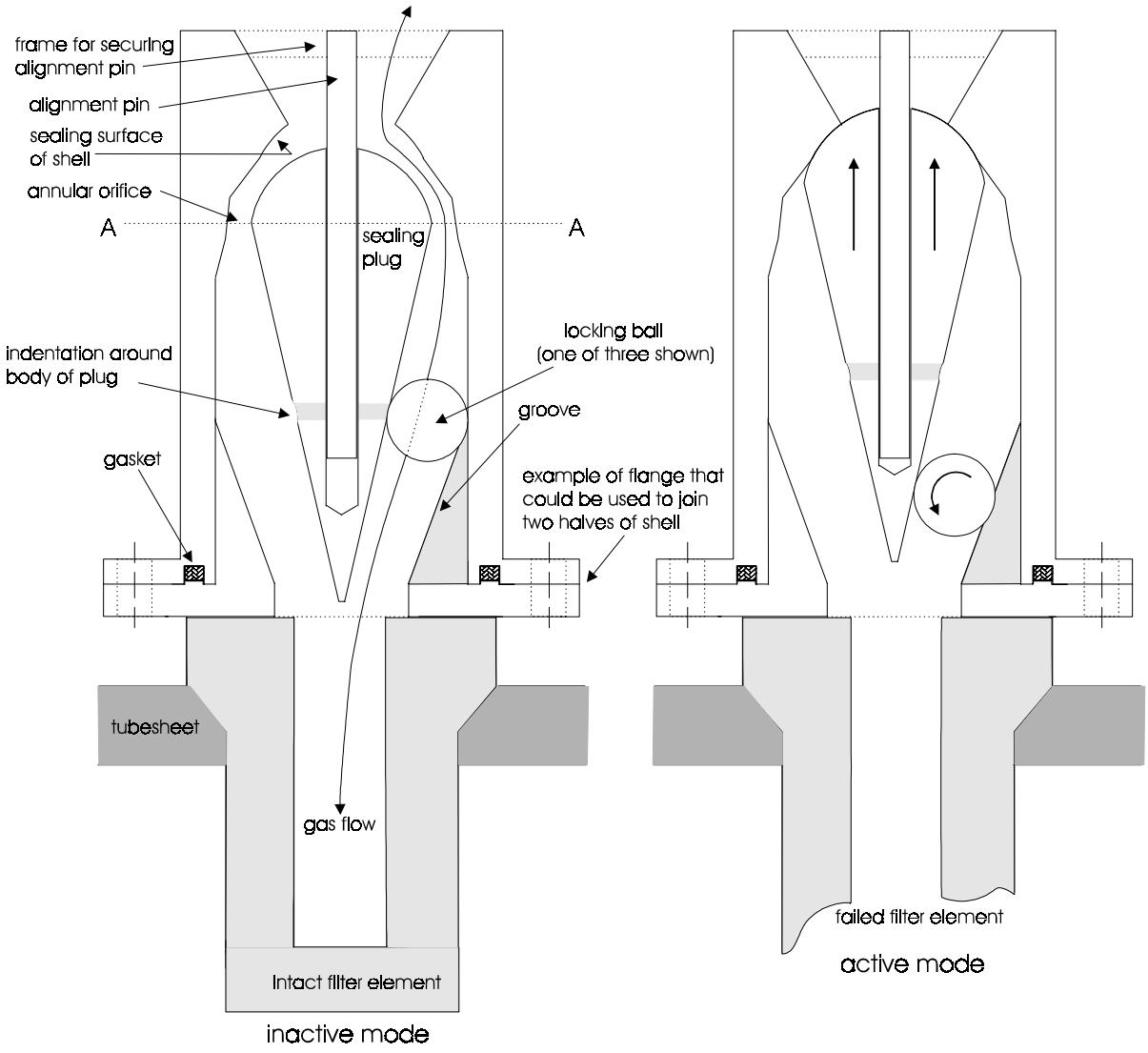

Figure 1. Schematic of FFMSGD operation illustrating the activation of the device when its candle filter undergoes catastrophic failure.

As shown in Figure 1, the exterior of the FFMSGD is typically a cylindrical shell; however, the external dimensions of the FFMSGD can be adapted to the tubesheet or hardware to which it must be attached. Centered holes in the top and bottom of the shell allow flue gas and pulse-cleaning gas to pass through the device. In the design used for P1 and P2, the top hole has a spherical sealing surface that is lapped during manufacture to mate with the spherical top surface of the sealing plug when the FFMSGD is activated. The form of the sealing plug is essentially a lower cone joined to a segment of a sphere at the upper, large end of the cone. The design weight of the sealing plug is established by the density of the material from which it is constructed. The sealing plug is supported by three spherical locking balls that in turn rest on a conical surface inside the lower portion of the shell. Grooves are cut into this conical surface under each ball to guide its movement when the FFMSGD is activated. A shallow spherical indentation around the circumference of the plug at the height where the balls contact the plug in the inactive mode helps to hold the plug and balls in their inactive positions during installation, and in the presence of normal vibrations that may be experienced in the filter vessel. In addition, these balls contact the inner wall of the shell to further secure them against vibration in the inactive mode.

The annular gaps between the plug and the various surfaces in the shell are sized so that the flow of filtered flue gas through them (when the filter element is intact) does not generate enough pressure drop to loft the sealing plug from its resting place on the three balls. By maintaining large enough annular flow paths for the movement of filtered flue gas and pulse-cleaning gas, an inactive FFMSGD will not add significant flow resistance to the filter system during either filtering or pulse-cleaning processes. The dimensions of the shell, the conical surfaces, the sealing plug and the balls determine the cross-sectional areas of the annular gaps between the plug and the shell. The FFMSGD is designed so that the smallest annular gap between the plug and the shell corresponds to the widest point in the plug (where the conical, lower portion of the plug mates with the top, spherical segment). This annular gap is designed to be large enough to assure that the sealing plug in the FFMSGD remains immobile when its candle filter element is intact. This same annular gap in the FFMSGD must also be small enough so that the increased flow experienced when its candle filter fails creates a pressure drop that is sufficient to loft the plug into its sealed position. Selecting the cross-sectional area of this gap provides the primary means of establishing the range of flows (and resulting pressure drops) for operation of the device. In addition, the weight of the sealing plug, the density of the gas, and a discharge coefficient (C_d) determine the conditions at which the FFMSGD will activate. (C_d and these other factors are discussed later in this report.)

The FFMSGD design includes a loose fitting alignment pin to ensure that the sealing plug does not tilt excessively during its short travel up to the sealing surface of the shell when the device activates. This guaranteed alignment assures that the lapped sealing surfaces will mate and form a good seal. It also assures that none of the three balls meant to lock the plug in place after activation can fall into the throat of the failed candle and possibly damage nearby filter elements, the hopper, or other downstream components of the ash disposal

system. Perfect vertical alignment of the sealing plug is not required for it to be held securely up against the sealing surface of the upper shell.

The long narrow taper of the conical, lower portions of the sealing plug and the shell are designed to prevent the forces exerted on the balls in active mode from causing them to slide back up the inner walls of the shell, thereby compromising the FFMSGD seal. Therefore the angle between these two cones has been kept small (< 14°), causing any downward force applied by reverse-gas cleaning pulses to the top of the plug, and subsequently to the locking balls to be transferred almost directly across the center of the balls to the wall of the shell. Therefore the locking balls will not be pressed up out of their activated positions by the intermittent downward force applied by the pulse gas.

The FFMSGD shell is designed in two pieces so it can be disassembled in order for the sealing plug and locking balls to be inserted. For the three prototypes manufactured and tested under this project, it was possible for the locking balls and the sealing plug to be properly positioned by hand. However, a small implement could be designed to aid in this procedure if a SGD with reduced size or a with a more difficult access was designed for a different installation or process. The installation of the FFMSGD requires proper care so that the sealing plug and balls do not become dislodged from their inactive positions.

PROOF-OF-CONCEPT FFMSGD TESTS

Initial laboratory experiments were conducted prior to designing the first prototype FFMSGD (P1) to measure the forces and flow velocities required to loft conical plugs somewhat like the sealing plug shown in Figure 1. These experiments were designed to estimate the discharge coefficient, C_d, for annular orifices. C_d is defined in Equation 1, which relates v, the velocity of gas through an orifice, and ρ, the density of the gas, to ΔP, the pressure drop across it.

$$\Delta P = \tfrac{1}{2}\, \rho (v/C_d)^2 \qquad (1)$$

An apparatus was constructed so that the upward flow of air through a vertical tube with an inner diameter of 2 inches could be adjusted. Two conical plugs with maximum diameters just under 2 inches were selected from available hardware. Measurements were made of the air velocity in the tube required to suspend each of the two plugs on the upwardly-flowing column of air. The pressure drop across the annular orifice between the plug and the tube was also measured to verify that this pressure drop equaled the weight of the plug divided by its maximum cross-sectional area. These measurements yielded values of 0.57 and 0.89 for C_d.

DESIGN OF THE PROOF-OF-CONCEPT FFMSGD PROTOTYPE

Based on the measurements of C_d, the test conditions established for the Task 1 laboratory bench-scale tests, and the objectives of these tests, the basic design of the first prototype FFMSGD (P1), as shown in Figure 2, was developed and submitted to a machine shop for fabrication.

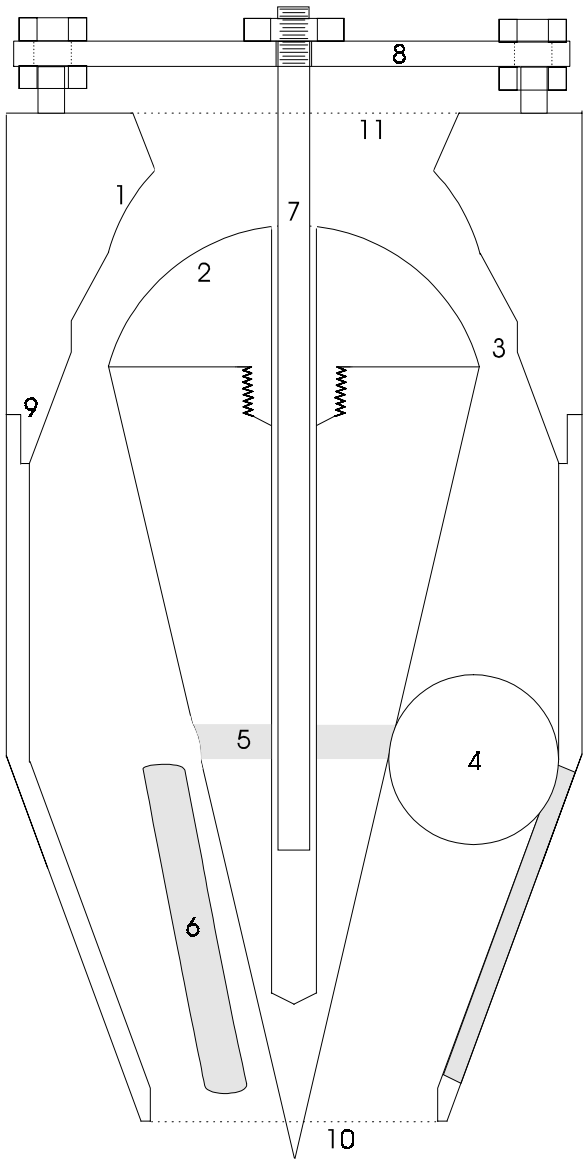

Figure 2. Schematic of the FFMSGD prototype used in the Task 1 laboratory bench-scale tests.

The FFMSGD uses a spherical sealing surface (items 1 and 2 on Figure 2). The cross-sectional area of the orifice (item 3) was set small enough to generate a sufficient pressure drop to loft the sealing plug when a filter element is broken, but large enough to minimize the pressure drop through the FFMSGD at a flow rate of about 30 acfm (when the candle filter element is intact). The dimension of the balls (item 4) used to support the sealing plug in the inactive mode, and lock the plug in position in active mode, was set at a diameter of 7/8 inch so commercially available balls could be used in the final design, and to minimize costs for the prototype. The three locking balls used in the laboratory evaluations of P1 were off-the-shelf items fabricated from silicon nitride. The lower section of the sealing plug is indented completely around its circumference (item 5) to provide the stability to withstand vibration without making installation unnecessarily difficult. For the prototype P1, the grooves (item 6) that guide the balls down to their locking positions are cut all the way though the lower wall of the shell to reduce fabrication costs. (The outer dimension of the entire lower portion of the shell was set to match the top portion of the shell in the later two prototype versions of the FFMSGD. Therefore these grooves were not be open to the outside of the shell in later versions of the device.) To prevent misalignment of the sealing plug as it is lofted to the sealing surface, the design of the FFMSGD included an alignment pin (item 7) and frame (item 8). The outer shell of prototype P1 was assembled with a simple slip fit (item 9) to reduce costs. The outer dimension of the FFMSGD P1 shell is 3 inches, which allowed easy integration with a clear acrylic mounting tube used in the bench-scale tests. The openings at the bottom (item 10) and top (item 11) of the FFMSGD were designed to be large enough to generate only a small obstruction to filter and pulse flows in the inactive mode. Except for the locking balls and the alignment pin, P1 was fabricated entirely from aluminum. The weight-to-volume ratio of the aluminum sealing plug (as compared with a 310 SS plug in the later prototypes) tends to compensate for the difference in the densities of laboratory air and typical HGCU process gas.

After P1 was received from the shop, two modifications were made to the original design. The 0.188” diameter alignment pin originally manufactured was replaced with a slightly larger (0.203”) diameter pin. The tighter tolerance between the pin and the 0.219” diameter shaft down the center of the sealing plug ensured a more vertical alignment of the plug as the device activated. Although the spacing between the alignment pin and the shaft was decreased by this change, the gap was still large enough to allow a loose fit, ensuring no significant resistance to the upward movement of the sealing plug during activation. The second modification to P1 was the introduction of a spacer between the two pieces of the sealing plug. (A large washer was used for this purpose.) This change increased the height of the sealing plug, thereby decreasing the conical spacing between the lower portion of the shell and the conical surface of the sealing plug when P1 was activated. This change was made to ensure that even in the worst case of misalignment of the sealing plug, no two locking balls would contact each other, and that there would be no possibility of any of the balls falling out of the device through the opening at the bottom of P1.

PROOF-OF-CONCEPT TEST OBJECTIVES

The FFMSGD concept is not merely a refinement of an existing system, but rather an innovative approach that depends on the quality of a mechanical seal and also on the movement and interaction of the sealing plug and the locking balls. For these reasons, the initial development of the FFMSGD has included two laboratory tests designed to verify that the concept has a good chance of success at harsh HGCU conditions. The first of these bench-scale tests was a simple evaluation of the freedom with which a horizontal 310 SS plate would release a silicon nitride ball that had been resting on the plate for an extended time in a high temperature environment.

Locking Ball Free Rolling Test

One of the 7/8 inch diameter silicon nitride locking balls was placed in a small dimple on a horizontal section of 310 SS plate and exposed to 1600 °F in a laboratory furnace. After about one week of contact with the plate at this elevated temperature the furnace was gradually inclined to determine if the ball would easily release from the surface of the plate and roll out of the dimple. The angle to which the furnace had to be inclined (approximately 10° from horizontal) to cause the ball to roll free was essentially the same angle that was needed for this test when performed at room temperature. This test indicates that no difficulties would be expected for operation of the locking balls in the safeguard device at oxidizing HGCU conditions. Other than some discoloration, both the 310 SS plate and the silicon nitride ball were not significantly affected by the extended exposure to 1600 °F. Although no high temperature laboratory evaluations were performed at reducing conditions, the successful use of 310 SS at the PSDF in reducing conditions and the predicted stability of silicon nitride in a reducing environment strongly suggested that the locking balls would also move freely in a gasification application.

Flow and Activation Tests

Flow and activation tests were performed to assess the performance of the prototype FFMSGD in four categories:

- pressure drop and device stability during inactive mode operation
- flows and pressure drops required to activate the device (with an evaluation of the integrity of the resulting seal in the *absence* of entrained ash)
- flows and pressure drops required to activate the device (with an evaluation of the integrity of the resulting seal in the *presence* of entrained ash)
- evaluation of the integrity of the seal made by the FFMSGD when subjected to reverse-gas pulses.

These evaluations were made using the P1 prototype at ambient temperature and pressure. The laboratory setup used for these evaluations is shown in Figure 3. The procedures followed to evaluate P1 are given in Table 1.

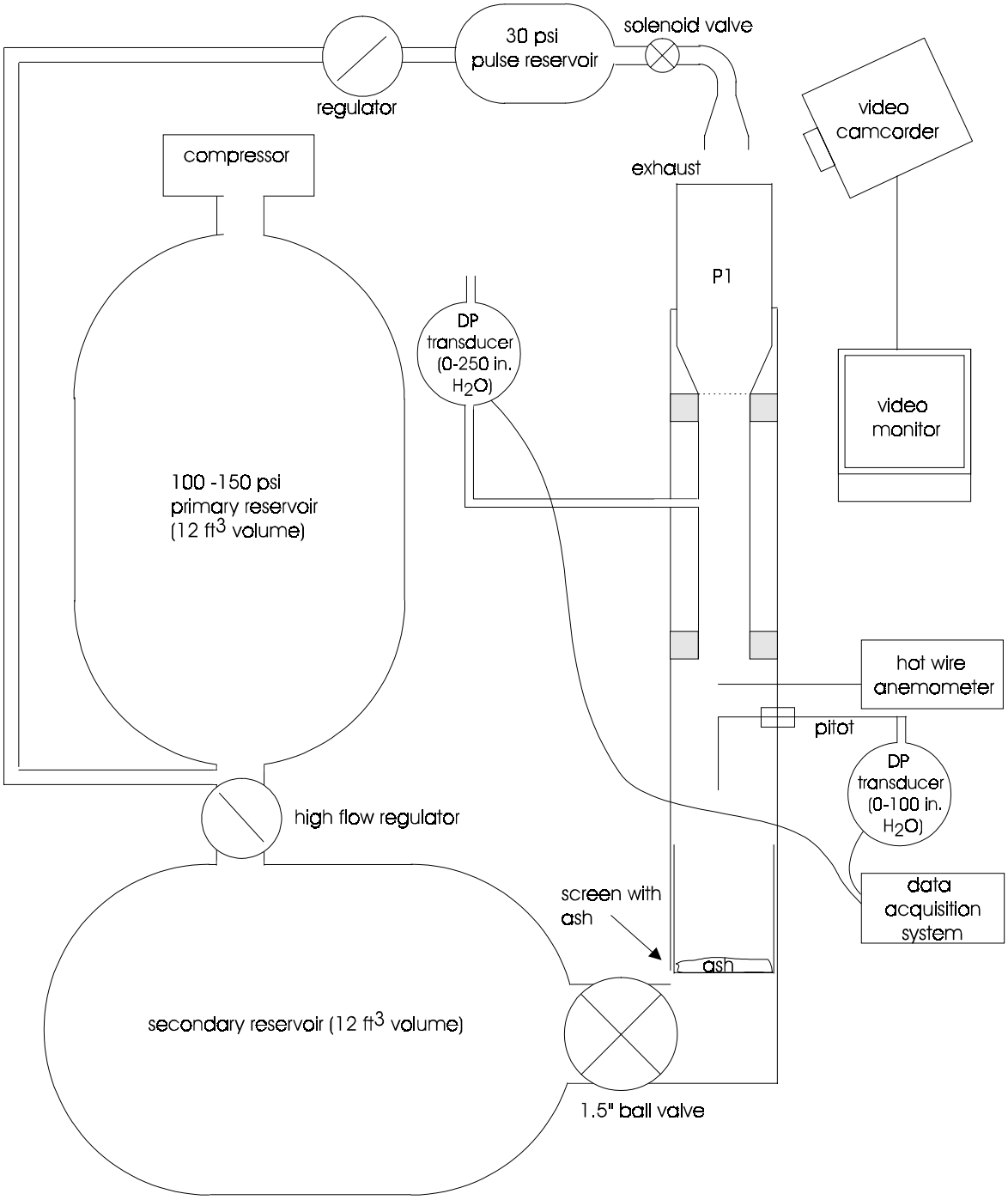

Figure 3. Setup used to evaluate P1 in bench-scale testing at Southern Research Institute.

Table 1
Test Procedures used to Evaluate P1

I. Verifying P1 Integrity and Operating Pressure Loss When a Candle is Intact
charge and maintain the pressure of the 100 psi primary reservoir
set the high flow regulator to 0 psi
start the data acquisition system and open the ball valve
adjust high flow regulator to generate 30 acfm in the acrylic tube (determine velocity with a pitot)
verify that the sealing plug does not dislodge
vibrate P1 while videotaping the position of the balls and sealing plug
measure and record the pressure drop across P1 during flow
charge the pulse reservoir to 30 psi
activate the solenoid to expose the top of P1 to reverse pulses
observe the position of the plug and the locking balls
repeat the last three steps several times
II. Verifying Activation and Integrity of the P1 Seal When the Candle Breaks
charge and maintain the pressure of the 100 psi primary reservoir
shut the ball valve and raise the pressure in the secondary reservoir to 1.8 psi (50 inches H_2O)
activate video camera, recorder and the data acquisition system
quickly open the ball valve to simulate the breaking of a candle (this should activate P1)
once P1 has activated, use a soap solution at its top surface to check for leaks
videotape this leak test and the position of the balls
vibrate P1 while leak checking it
pressurize the upstream side of the activated P1 to just over 100 inches H_2O
close the ball valve and monitor the pressure upstream of P1 as a function of time
vibrate P1 while monitoring the pressure upstream of P1 as a function of time
III. Verifying Integrity of the P1 Seal During Reverse Pulses
activate P1 as in test II above
charge the pulse reservoir to 30 psi
activate the solenoid to expose the top of P1 to reverse pulses
observe the position of the plug
repeat the last three steps several times
IV. Verifying Activation and Integrity of the P1 Seal as Formed with Entrained Dust
charge and maintain the pressure of the 100 psi primary reservoir
insert the screen in the tube below P1 and position ash on the screen
shut the ball valve and raise the pressure in secondary reservoir to 1.8 psi (50 inches H_2O)
activate video camera, recorder and the data acquisition system
quickly open the ball valve to simulate the breaking of a candle
when P1 activates, shut the ball valve and leak check the top surface of P1 with soap solution
videotape the leak check test and the position of the balls
pressurize the upstream side of the activated P1 to 100 inches H_2O
close the ball valve
monitor the pressure upstream of the SGD as a function of time
vibrate P1 while monitoring the pressure upstream of P1 as a function of time

At ambient temperature and pressure, the air passing through P1 during these bench-scale tests had a nominal density of about 1.2 kg/m^3, and a viscosity of about 184 poise. These values differ from those of flue gas at typical HGCU conditions (e.g. 10 atm and 1600 °F). At these HGCU conditions the safeguard device would be operating with gas having a density of about 3.1 kg/m^3 and a viscosity of about 455 poise. The effects of the increased density of the gas at HGCU conditions (a factor of X 2.6) are essentially offset by the higher density of the 310 SS that was used to construct latter two high-temperature prototypes versus the density of the density of the aluminum used to construct P1 (a factor of X 2.9). Any effects of the increased viscosity of the gas at HGCU conditions compared with the results obtained at room temperature was expected to be negligible because the safeguard device acts essentially like an orifice. (Viscosity does not affect the pressure loss incurred as gas passes through an orifice.)

For the purposes of the laboratory evaluations, the normal flow through P1 was set to correspond to that which would be experienced by a safeguard device located on a 1.5 meter candle filter element filtering gas at an actual filter face velocity of 10 feet per minute. For the purposes of quantifying the leak rate across P1 once it had been activated, a pressure behind the seal (corresponding to the tubesheet pressure drop) of 100 inches H_2O was selected.

The pressure drop through P1 at normal flow (30 acfm - which corresponds to an intact filter element operating with a face velocity of 10 actual feet per minute) was measured to be about 1.5 inches H_2O. As P1 was exposed to gradually increasing flows, the pressure drop across P1 eventually reached about 8 inches H_2O (at a flow rate of about 69 acfm), at which time the device activated. This activation can be seen in the data presented in Figure 4. The measured value of ΔP required to activate P1 was 8 inches H_2O. The flow rate required to activate P1 was 69 acfm. Based on the mass of the sealing plug as tested (275 g), and its cross-sectional area at its widest point (about 19.1 cm^2), the pressure required to lift the plug (with $C_d = 1.0$) should be only 5.7 inches of H_2O. The excess pressure required to activate P1 in the laboratory evaluations (8 - 5.7 = 2.3 inches H_2O) represents the pressure lost as the gas passed around the locking balls and through the openings at the inlet and outlet of the shell combined with the effects of the discharge coefficient.

The speed with which P1 activated was assessed in a separate test by suddenly exposing the inactive device to a pulse of air stored in the secondary reservoir. Based on visual and videotaped examination of these trials, P1 activated about 0.3 seconds after the pulse of air was released by opening the 1.5 inch ball valve called out in Figure 3. P1 formed a high quality seal each time it was activated. The seal formed by P1 activated without entrained ash and with 100 inches of back pressure leaked approximately 0.11 acfm. Another way to express this leak rate is that activating P1 would stop 99.6 % of the nominal gas flow (30 acfm) for a broken filter element location that had been filtering gas (prior to activation of the safeguard device) at a face velocity of 10 feet per minute with a tubesheet pressure drop of 100 inches H_2O. Measurements of the leak rate through an activated seal formed with

entrained ash yielded similar, but slightly better, results. The seal formed by P1 activated with entrained ash and with 100 inches of back pressure leaked approximately 0.08 acfm. This equates to stopping 99.7 % of the nominal gas flow (30 acfm) for a broken filter element location that had been filtering gas (prior to activation of the safeguard device) at a face velocity of 10 feet per minute with a tubesheet pressure drop of 100 inches H_2O. It is important to note that these are gas leak rates. Because the leak paths along the sealing surface formed between the sealing plug and the upper shell are composed of very fine crevices, the ash particles that are carried to these leak paths are expected to rapidly deposit and bridge over the inlet to these crevices. This should cause the quality of the seal to improve for the capture of gas and also establish a particle collection efficiency of essentially 100 %. Alternative safeguard devices that depend on pore plugging rely on this mechanism to trap particles in passages that allow gas flow in the inactive mode.

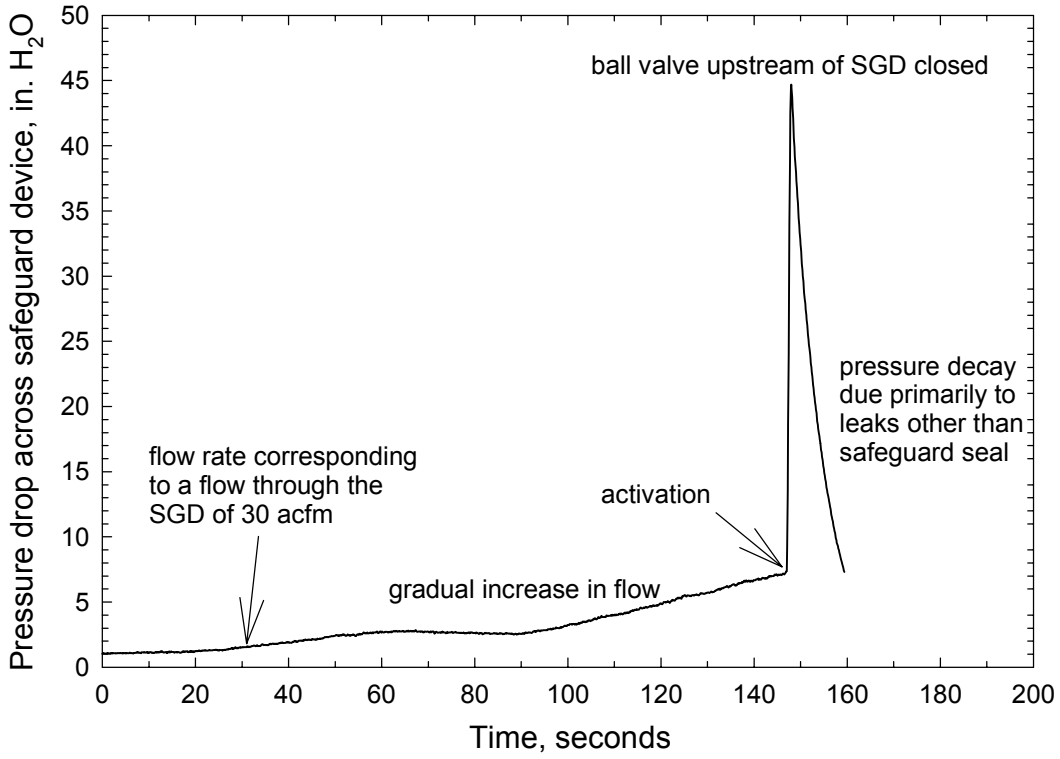

Figure 4. Activation of P1 induced by a gradual increase in flow. Activation occurred at a flow rate of about 69 acfm.

Discussions with Zal Sanjana of Siemens Westinghouse indicated that a pulse pressure of 30 psi would be the highest value that could be expected to reach the top of the safeguard device in their filter design. Therefore P1 was exposed to pulses of 30 psi discharged from a fast acting solenoid valve through a 1.5 inch diameter pipe centered and suspended about two inches above the sealing surface of the device. Repeated pulses had no effect on the position of the sealing plug and the locking balls in the inactive mode. After activating the device with a sudden pulse of air from the upstream side, P1 was again exposed to repeated 30 psi pulses. None of these reverse-cleaning pulses visibly moved the sealing plug from its activated position or degraded the pressure seal formed during activation.

PILOT-SCALE FFMSGD TESTS

Pilot-scale tests at HTHP conditions were performed as an integral part of the demonstration of the FFMSGD technology. The first set of pilot-scale tests were performed with the second prototype FFMSGD in the Small Pressure Vessel (SPV) at the DOE High-Temperature Gas-Stream Cleanup Test Facility (HTGSCTF). These tests, which are discussed in the following sections, evaluated a variety of aspects of the performance of the FFMSGD. DOE's test facility allowed P2 to be tested at temperatures exceeding 1500 °F and at pressures around 70 psig. PFBC ash was reinjected into the SPV to assess the ability of the FFMSGD to prevent the passage of entrained ash particles across the tubesheet. As discussed below, these tests demonstrated that the prototype FFMSGD was able to meet all the objectives that could be assessed in DOE's test facility.

At the time of the preparation of this Final Report, the second set of pilot-scale tests are ongoing at the PSDF. These tests, which are also discussed later in this report, provide a realistic evaluation of the ability of the third prototype FFMSGD, P3, to withstand the reducing environment and HTHP conditions currently present in the HGCU filter at the PSDF (around 750 °F, and pressures around 220 psig).

In both of these sets of pilot-scale tests, the arrangement, schedules, costs, and the presence of hazardous conditions inherent in an HGCU filter created some limitations for an exhaustive evaluation of the FFMSGD technology. At the DOE facility, long-term exposure of the prototype to HTHP conditions was limited by the daily schedule at the facility and other work that had to be accomplished at the facility. Although the DOE facility could produce suitable temperatures and pressures, actual flue gas was not available. Also, the measurement of outlet mass concentrations was limited at the DOE facility, primarily because there are few, if any, monitors that can reliably and accurately make measurements of entrained particulate matter at concentrations near 1 ppm in HTHP environments.

Although the ongoing tests at the PSDF provide some additional capabilities when compared with the DOE pilot-scale tests, there are also some extra limitations associated with the FFMSGD evaluation at the PSDF. The primary limitation is test scheduling. Because the PSDF involves many advanced components and multiple parallel evaluations, the evaluation of the FFMSGD is subject to the schedule dictated by these other factors. Because the PSDF HGCU filter must be able to support the overall PSDF test run, its configuration and overall operation can only be slightly altered to allow for the FFMSGD evaluation. The advantages of the PSDF evaluation include extensive exposure to actual, rather than simulated, HTHP environmental conditions. The PSDF evaluation will also potentially expose the FFMSGD to system shutdowns and restarts, system upsets, temperature excursions, and vibrations of the HGCU filter vessel.

DESIGN OF THE INITIAL FFMSGD PROTOTYPE FOR HTHP OPERATION

The design of P2 was adapted from the design of the first prototype to match the dimensions and constraints of the SPV. In general, the internal dimensions of P2 matched those of P1, except that the solid volume of the sealing plug in P2 was reduced by removing some of the material inside the plug. This was done to adjust the weight of the plug to compensate for the difference in gas density for the tests to be conducted at HTHP conditions. (Because the density of the gas in the SPV at 70 psig and 1500 °F would be about 1.5 times the density of the air at ambient temperature and ambient pressure when P1 was tested, enough material was removed from the interior volume of the P2 sealing plug to cause its weight to be about 1.5 times the weight of the P1 sealing plug.

(Material had to be *removed* from the P2 plug design to compensate for the differences between the ratio of the densities of the materials used to construct P1 (aluminum) and P2 (310 SS) and the ratio of the densities of the ambient air used during the P1 evaluation and the HTHP gas to be used for the P2 evaluation.) Although features of P2 such as the cross-sectional area of the annular orifice around the widest point in the sealing plug (1.14 in^2) or the shape of the interior walls of the shell could have been modified from the specifications used to construct P1, the decision was made to hold as many of these dimensions constant between these two prototypes as possible. This consistency was maintained in case there was a need to make direct comparisons between data obtained for P1 and P2. Another minor change was that the diameter of the alignment pin was increased to make it stronger and easier to properly align on the central axis of the device. Figures 5 through 8 present photographs of P2 assembled and in various states of disassembly prior to its installation in the SPV. Figure 9 presents a cutaway illustration of P2, with one of the three locking balls shown in its position when inactive (darker ball in foreground) and in its position when P2 has activated (lighter ball in the background).

Figure 5. Complete P2 assembly.

Figure 6. P2 sealing plug and locking balls.

Figure 7. Sealing plug in its inactive position supported on the three locking balls positioned in the lower shell.

Figure 8. Lower shell showing the vertical channels used to maintain the 120° spacing of the three locking balls during activation.

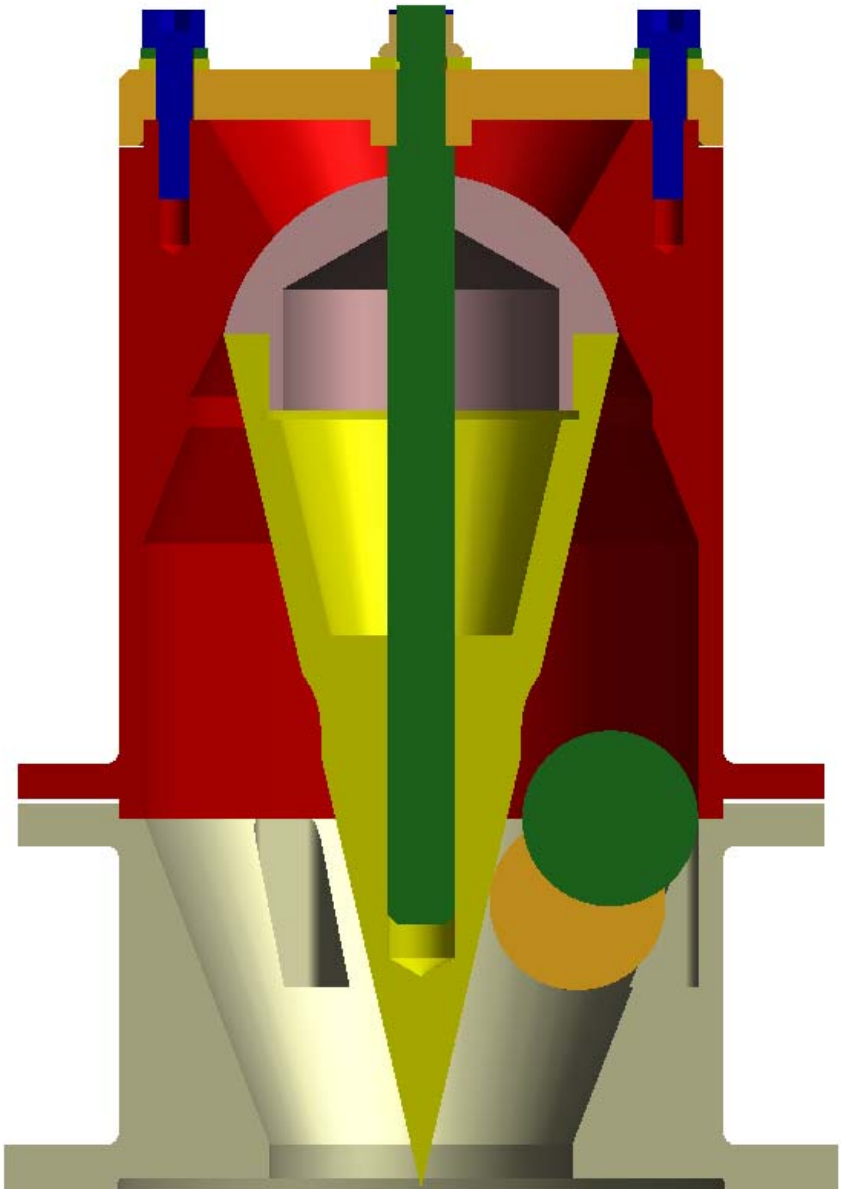

Figure 9. Cutaway view of P2, with one of the three locking balls shown in its position when inactive (darker ball in foreground) and in its position when P2 has activated (lighter ball in the background).

The material selected for the construction of P2 was 310 stainless steel (aluminum was used for P1). In evaluations performed at the Power Systems Development Facility (PSDF), 310 SS has been shown to be the most durable material for duty in oxidizing and reducing environments. 310 SS is also easily machined. The locking balls incorporated into the design of P2 are constructed from silicon nitride (Si_3N_4), which is also durable in oxidizing and reducing environments. (The choice to use Si_3N_4 for the locking balls for P2 was made to hold down costs. Because of some minor effects resulting from differences in the coefficients of linear expansion of Si_3N_4 and 310 SS which are discussed later in this report, the locking balls should be fabricated from 310 SS in fully mature designs. 310 SS balls are not currently offered without special ordering. However, ordered in sufficient quantities for a full-scale filter vessel the ultimate cost of 310 SS balls should be lower than Si_3N_4 balls.) The gaskets used to secure the FFMSGD to the filter element and the existing SPV tubesheet were of the same type currently used at the SPV. The external features of P2 were designed to allow the FFMSGD to be bolted together with a flange about halfway up its outer shell. The two portions of the shell are joined with flat, machined surfaces designed to provide a metal-to-metal seal at their plane of contact when the external flanges are bolted together. The bottom portion of the shell was adapted to bolt directly to the SPV tubesheet in the same way as the conventional hold-down plates used with the SPV tubesheet.

TEST OBJECTIVES

The general objectives for an effective SGD are discussed in the section on performance criteria at the beginning of this report. The specific objectives of the tests of P2 are listed in Table 2.

Table 2
Objectives of the HTHP Characterization of the SRI FFMSGD in the DOE HTGSCTF

#	description
1	Quantify the conditions required to activate the FFMSGD during ambient temperature operation.
2	Quantify the conditions required to activate the FFMSGD during HTHP operation.
3	Determine the ability of the inactive FFMSGD to withstand repeated reverse-gas pulses.
4	Determine the ability of the activated FFMSGD to withstand repeated reverse-gas pulses.
5	Assess the degree to which activation of the FFMSGD during HTHP operation provides a barrier to the transport of entrained ash across the tubesheet.
6	Quantify the effect of the inactive FFMSGD on pulse cleaning.

Objectives 1 and 2 in Table 2 were addressed by determining the temperature and density of the gas entering the FFMSGD, and the velocity of the gas as it passed through the FFMSGD. The configurations of the tubesheet, filter elements and the FFMSGD, and the types and locations of sensors attached to the SPV did not allow direct measurement of the gas temperature and velocity entering the FFMSGD in the HTHP tests. Estimates of these quantities and the gas density were based on gas flow entering the SPV, and gas temperature below the tubesheet (in the SPV). These estimates also had to take into account any changes in the SPV internal pressure that were occurring at the time of activation. Except in the case when the FFMSGD activated as a result of filter element failure (discussed later in this report) activation of the FFMSGD was clearly indicated by a sudden increase in the tubesheet pressure drop.

For objective 3, clear indications of the ability P2 to withstand reverse-gas cleaning pulses in its inactive mode were provided in run 17 (discussed in detail later in this report) when, after experiencing seven filtration and cleaning cycles, P2 activated immediately after the failure of its filter element. With respect to objective 4, observations of the tubesheet pressure drop traces following repeated reverse-gas cleaning pulses directed at the top of the activated FMSGD provided the primary indication of whether these pulses disturbed the device. Measurements of outlet mass levels provided by the PCME device (discussed in detail later in this report) also provided indications of the ability of the activated SGD to withstand reverse-gas cleaning pulses.

Objective 5 was addressed through post-test inspections of the appearance of the seal formed when P2 activated, and by examination of the readings provided by the PCME in the outlet piping. These observations and data are discussed in detail in the body of this report.

The quantification of the effect of the inactive FFMSGD on pulse cleaning, was intended to be achieved in run 17. However, the failure of the filter element under the SGD during this run (presumably due to the thermal and/or mechanical stresses placed on it by the reverse-gas cleaning pulses), caused this objective to be abandoned. This event is discussed in detail in the body of this report.

TEST PLAN

The test plan used for the evaluation of P2 is summarized in Table 3.

Table 3
Overview of Plans for Assessment of P2 Performance

activity	addresses objective
characterize the flows and pressure drops associated with activation of P2 at ambient temperature and ambient pressure at SRI's laboratory	1
characterize the flows and pressure drops associated with activation of P2 at ambient temperature and low and medium pressures in the SPV	1,2
characterize the flows and pressure drops associated with activation of P2 at HTHP conditions in the SPV	2
expose P2 (inactive) to repeated reverse-gas pulses at HTHP conditions	3
expose P2 (activated at HTHP conditions) to repeated reverse-gas pulses at HTHP conditions	4
obtain baseline PCME signal levels (with P2 activated at HTHP conditions) prior to ash injection	5
obtain baseline PCME signal levels (with P2 activated at HTHP conditions) following ash injection	4,5
record pressure drop during repeated filtration and cleaning cycles for a filter element fitted with P2 (inactive) along side a second element with no SGD	3,6

LOW TEMPERATURE EVALUATION AT SRI

Prior to designing the details of the conditions for the SPV tests, a limited series of tests were conducted at SRI's laboratories in Birmingham to determine the flow required to activate P2 at ambient temperature and pressure, and to measure the pressure drop across P2 as a function of flow rate up to and including the point of activation. The setup used for these measurements is shown in Figure 10. It is important to note that because the setup used at SRI incorporated a smooth flow transform into the body of P2, it was possible to position a pressure tap so that the pressure drop across P2 only could be measured. (In the SPV tests, the values of tubesheet pressure drop measured included pressure drop incurred in the transform from the SPV pressure vessel into the body of P2, as well as pressure drop incurred as the gas passed through P2. This is discussed in more detail later in this report.)

Data obtained in the flow tests performed at SRI are presented in Figures 11 and 12. P2 activated at a flow of 107.5 acfm (a velocity through the annular orifice of 69 m/s), and a ΔP across the device of 11.2 in. H_2O. In order to compare the data obtained at these ambient conditions at SRI's laboratory with similar data obtained at the SPV at various conditions, a lift factor, ρv^2, was calculated according to the definition presented in Equation 2:

$$\text{lift factor} = \rho v^2 \quad (2)$$

where ρ = the gas density, kg/m^3

v = the actual velocity of the gas through the annular orifice of P2, m/s.

For the test data shown in Figures 7 and 8, the lift factor at the point of activation was about 5,800 kg/ms^2.

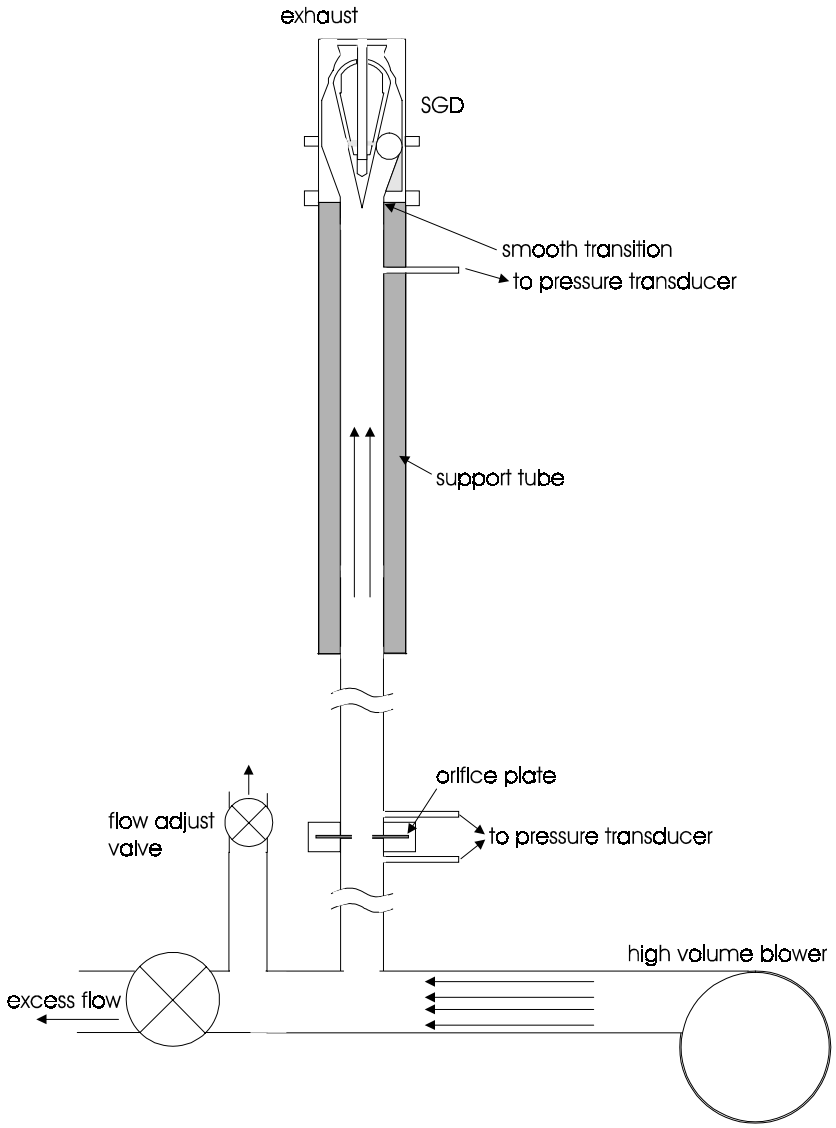

Figure 10. Setup used to evaluate P2 in bench-scale testing at Southern Research Institute.

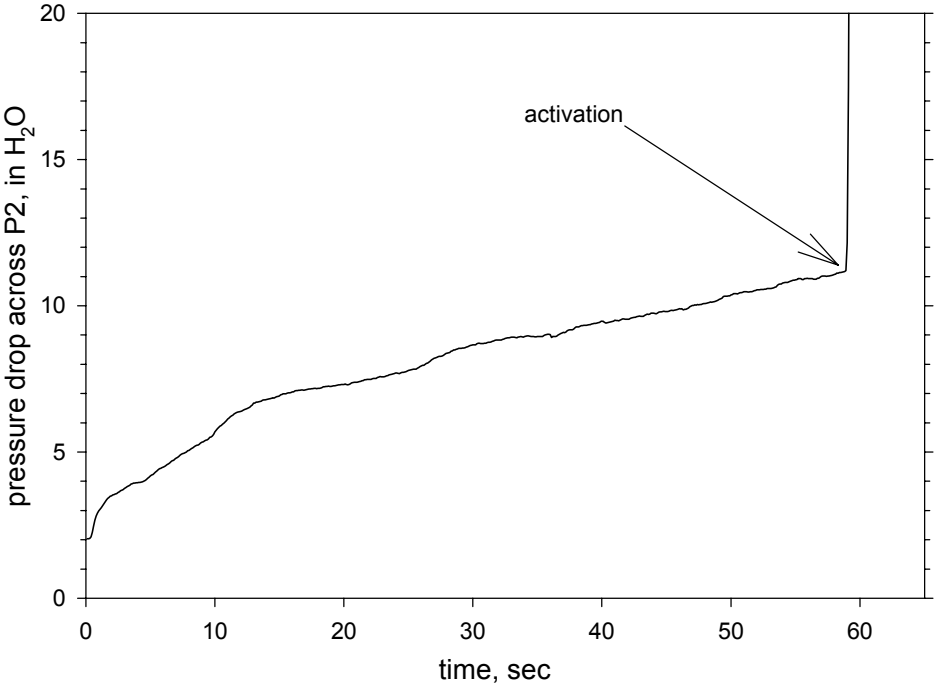

Figure 11. Pressure drop across P2 as flow through it was manually increased until it activated.

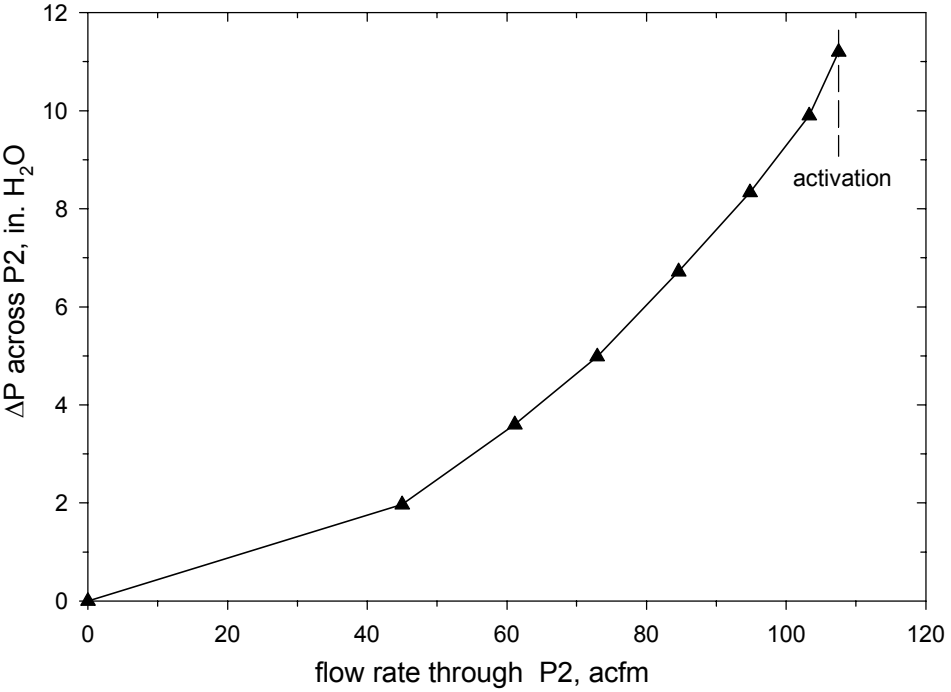

Figure 12. Pressure drop across P2 as a function of the flow rate through it.

PILOT-SCALE TESTING AT THE DOE/NETL SPV

The evaluations of the performance of P2 at the SPV were intended to meet the six objectives stated in Table 1. Because these objectives concerned different SGD performance criteria, the evaluations in the SPV were divided into tests runs that addressed different aspects of the operation of P2. The timing and configurations of these individual tests were selected to minimize the time that the DOE High-Temperature Gas-Stream Cleanup Test Facility (HTGSCTF) would be occupied with the evaluation of P2. Other constraints on the tests performed at the SPV included safety concerns (discussed below), time required to heat the system to the target temperature of 1500 to 1550 °F, time required to cool down the system to change the test configuration, the potential to contaminate the region downstream of the tubesheet with ash after ash was injected for the first time, the flow capacity and total filter area available in the SPV system, as well as limits on the operation of the back pressure relief valve. Safety concerns were the primary reason that the plans for the evaluation of P2 did not include the breaking of a filter element during HTHP operation. It was determined that all methods proposed for triggering a filter element failure at HTHP conditions could expose the SPV operators to extreme hazards. (However, the filter element did inadvertently break during run 17, providing very valuable information about the ability of P2 to activate in case of filter element failure. This event is discussed in detail later in this report.) Based on the constraints mentioned above, and other factors related to the design of the HTGSCTF / SPV system, a series of test runs was performed between June 5 and June 23, 2000, and also on July 12 -13, 2000. A summary of these test runs and discussion of the data obtained are presented following a brief description of the DOE/NETL HTGSCTF and SPV, which was drawn from information presented in RFP No. DE-RP26-99FT40199.

The operating conditions at which P2 was evaluated at the DOE/NETL HTGSCTF were selected to be as harsh and rigorous as possible. Therefore the normal filtering face velocity was set to be 10 acfm/ft^2 (10 ft/min), the system temperature selected for the high-temperature tests was always as high as the system and schedule would allow (usually around 1500 °F, although some tests were performed at 1550 °F), and the surge tank (which supplied the reverse-gas cleaning pulses) was pressurized to 350 psig (the maximum value used in any prior SPV testing by DOE).

Description of the DOE/NETL HTGSCTF and SPV

In support of DOE/NETL's hot-gas filter development program, the high-temperature, gas-stream cleanup test facility was designed to investigate conventional and novel approaches to high-temperature filtration, conduct detailed parametric studies that characterize particulate control devices under well-controlled oxidizing conditions, and screen new materials for other high-temperature applications, such as heat exchanger tubes. This test facility utilizes a natural gas-fueled combustor to produce high-temperature process gas, and a screw feeder to inject fly ash, or other fine particulate, into the gas stream to simulate process particle loading.

The pressure vessels that house the particulate control devices used in these evaluations have inside diameters of approximately 0.20 meters (8 inches) and 0.90 meters (34 inches) respectively. Three commercial-size filter elements can be tested simultaneously in the SPV. The facility is capable of operating over a wide range of conditions. Operating temperature can vary from 540 to 870 °C (1000 to 1600 °F), and the operating pressure can vary from 0 to 580 kPa (0 to 70 psig).

Figure 13 presents the schematic of the SPV HTGSCTF. The major components consist of the SPV, the combustor, the dust feeder and the back-pulse surge tank. The SPV is a carbon steel vessel with refractory lining. Its internal-working dimension is 0.20 meters (8 inches) in diameter by 2.61 meters (8 feet 9 inches) in height. A water-cooled, removable tube sheet divides the SPV into clean-gas and dirty-gas compartments. In the dirty-gas compartment, a maximum of three commercial-size candle filter elements (60 mm OD by 1.5 m long) can be attached to the tube sheet at a center-to-center spacing of 76-mm (3 inches). The three locations where these elements can be installed are labeled A, B, and C. In each test that P2 was installed on the tubesheet, it was placed in position B. This was done to provide the maximum room above the tubesheet for a back pulse tube to be installed over the SGD. In the clean-air compartment, three back-pulse tubes are positioned at the center of and just above each candle filter element. The clean-air compartment has a working volume of 0.20 meters (8 inches) by 0.28 meters (11 inches) height before reaching the exit nozzle. The exit nozzle can be removed to facilitate filter installation and back-pulse tube adjustment.

The process gas together with the entrained particulate matter enters the SPV from a bottom inlet and turns upward to the filter elements. The gas flow path passes through the filter elements, the tube sheet, and the exit nozzle. After leaving the SPV, the flow is cooled down with nitrogen/or water before it is exhausted to the atmosphere. Operating flow rate (measured prior to entering the SPV) can vary from 2000 to 9000 scfh (57 to 255 standard cubic meters per hour), depending on the filters under test, particle size distributions and particle loading. During filter regeneration, the back pulse dislodges the filter cake. The dislodged filter cake falls by gravity to the hopper below.

Natural gas with a primary air stream is mixed and combusted to produce a hot gas stream temperature up to 3000 °F (1700 °C). A secondary air stream is added to reduce the temperature to the sub 1900 °F (1090 °C) range. This allows fly ash to be injected without the possibility of ash fusion. The ash is input by a K-tron screw feeder with a loss-of-weight control system and conveyed by a nitrogen gas stream into a spool piece prior to the filter vessel. Particulate feed rate can vary from 2 to 50 lbs/hr to produce a simulated particle loading of 3000 to 20,000 ppmw at varying gas flow rates. A PCME particulate emissions analyzer with a medium temperature sensor at the SPV outlet is installed for on-line, real-time particle loading monitoring after the filters. Particle loadings from below 0.02 mg/m^3 to 1000 mg/m^3 (0.016 to 775 ppmw) are reported to be successfully monitored by PCME sensors.

The SPV HTGSCTF is monitored by a data collection and control system built around individual data collection modules and Paragon TNT data collection software. Data are collected by OPTO-22 data modules. Each of these modules has its own analog-to-digital converter and communicates data at rates around 10 Hz. A "brain board" or processor capable of spanning and linearizing signals connects these modules. The brain board communicates with a PC running Paragon TNT software for data collection, graphical operator interface and selected operating controls. To reduce data file storage needs, measured data are recorded by the Paragon TNT software only when the values change by a preset percentage. (This effect can be observed in the detailed run data presented later in this report.) Moore process controllers provide PID loop control for the flow loops such as primary air, secondary air, natural gas and conveying nitrogen for the ash. Relay logic is used for safety controls. Pressure measurements are primarily made by Rosemount smart transmitters, which have a frequency response of 10 Hz. These units are repeatable and calibrated to 0.15%. The unit is on a one-year calibration schedule. Process variables recorded include clean- and dirty-side pressure and temperature, flow rate, pressure inside the filters and differential pressure across the filters.

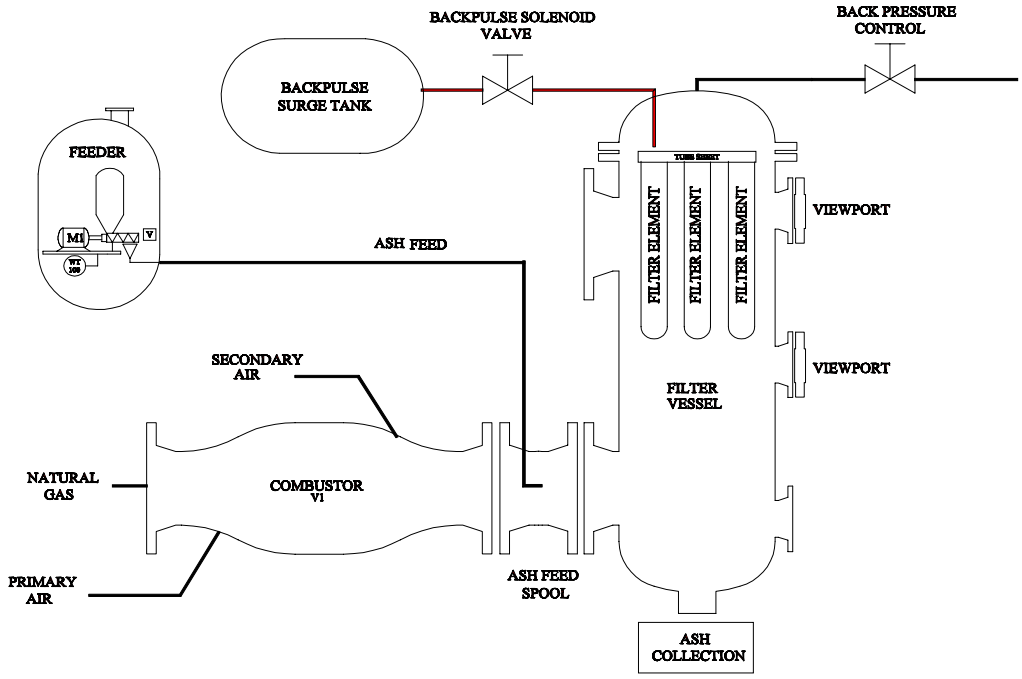

Figure 13. Schematic of the DOE/NETL HTGSCTF (the large pressure vessel is not shown).

Summary of SPV Test Runs

Table 4 provides an overview of the test runs made at the SPV during the evaluation of P2.

Table 4
Description of SPV Test Runs

run # / date	objective	events	comments
1 / June 6	cold activation (SPV exit nozzle on)	SGD did not activate (7.7 in. H_2O max. tubesheet ΔP)	filter elements and 3/4" orifices at A, C. SGD installed at B (over candle stub)
2 / June 6	cold activation (SPV exit nozzle on)	SGD did not activate (16.8 in. H_2O max. tubesheet ΔP)	filter elements and 3/8" orifices at A, C. SGD installed at B (over candle stub)
3 / June 6	cold activation (SPV exit nozzle on)	SGD did not activate (21 in. H_2O max. tubesheet ΔP)	filter element and 3/8" orifice at A, blank at C, SGD at B (over candle stub)
4 / June 6	cold activation (SPV exit nozzle on)	SGD activated (at 17 in. H_2O tubesheet ΔP)	filter element and 3/8" orifice at A, blank at C, SGD at B (candle stub removed)
5 / June 7	cold activation (SPV exit nozzle on)	SGD did not activate (21.6 in. H_2O max. tubesheet ΔP)	3/8" orifice at A, blank at C, SGD at B (candle stub removed) (repeat of run 4 conditions)
6 / June 7	measure ΔP of transition of flow from SPV vessel through single tubesheet opening	2.3 in. H_2O tubesheet ΔP at max. flow available to SPV (37 acfm)	blanks at A, C, no hardware or SGD at B
7 / June 7	cold activation (SPV exit nozzle on) (increase flow quickly)	SGD did not activate (24.8 in. H_2O max. tubesheet ΔP)	3/8" orifice at A, blank at C, SGD at B (candle stub removed) (repeat of run 4 conditions)
8 / June 9	exposed manually activated SGD to reverse gas pulses at HTHP conditions	pulsed top of SGD 15 times and noted PCME output (no ash injected prior to, or during, this run)	SGD withstood multiple reverse gas pulses, PCME showed a baseline reading about 0.16 to 0.30
9 / June 12	cold activation (SPV exit nozzle off)	slowly raised flow to max. and tubesheet ΔP reached 49 in. H_2O but SGD did not activate	3/8" orifice at A, blank at C, SGD at B (over candle stub)
10 / June 12	cold activation (SPV exit nozzle off)	quickly raised flow to max. and tubesheet ΔP reached 45 in. H_2O and the SGD activated	3/8" orifice at A, blank at C, SGD at B (over candle stub)

Table 4 (continued)

run # / date	objective	events	comments
11 / June 12	cold activation (SPV exit nozzle off) measure ΔP vs. flow for 3/8" orifice only	quickly raised flow to max. and tubesheet ΔP reached 32 in. H_2O and the SGD activated	3/8" orifice at A, blank at C, SGD at B (over candle stub) 3/8" orifice at A takes 20% of flow when SGD at B is open
12 / June 12	measure ΔP for all hardware (and candle stub) below entry into SGD	flow vs. tubesheet ΔP showed 20 in. H_2O at max. flow	bottom half of SGD over the candle stub at B, blanks at A, C
13 / June 12	measure ΔP for all hardware below entry into SGD	flow vs. tubesheet ΔP showed 12.7 in. H_2O at max. flow	bottom half of SGD (no candle stub) at B, blanks at A, C
14 / June 13	hot activation of SGD at max. temperature and minimum allowable pressure	SGD activated at a tubesheet ΔP of 20 in. H_2O, 1650 °F inlet temperature, system pressure of 54.3 psig	3/8" orifice at A, blank at C, SGD at B (over candle stub)
15 / June 14	expose SGD activated at HTHP conditions to reverse gas pulses with and without ash injection	continuing setup from the conclusion of run 14 - pulsed top of the SGD 15 times and noted PCME output (prior to ash injection) and pulsed locations A and B repeatedly during ash injection and filtration	SGD withstood multiple reverse gas pulses, PCME showed baseline around 0.2. Periodic spikes in PCME readings apparently caused by minor ash contamination above the tubesheet not related to the SGD seal
16 / June 20	get PCME baseline for a "perfect" SGD (a blank plate at B)	repeated activities of run 15	post test inspection revealed a crack in element at A, significant contamination above the tubesheet invalidated PCME baseline data
17 / June 22	expose the inactive SGD to reverse-gas pulses; assess relative effectiveness of cleaning through open SGD	inactive SGD withstood seven filtration / pulse cleaning cycles then its filter element broke and the SGD activated	element failure most probably caused by vigorous cleaning pulse. The filter element at A also broke at conclusion of run
18 / July 13	get PCME baseline for a "perfect" SGD (a blank plate at B)	repeated activities of runs 15 and 16	PCME showed baseline around 0.02. Periodic spikes in PCME readings apparently caused by minor ash contamination above the tubesheet

Low Temperature Operation

Low temperature evaluations of P2 (test runs 1 - 7, and 9 - 13 listed in Table 4) were performed in the SPV at elevated and ambient pressure levels. The objectives of these tests were to determine

- how P2 interfaced with the SPV
- whether or not the HTGSCTF could deliver sufficient flow to activate P2
- the effect of gas pressure on activation of P2
- identify the threshold value of the lifting factor needed to activate P2
- how the HTGSCTF control system would react to the sudden increase in tubesheet pressure drop when P2 activated
- flow vs. pressure drop for P2 in the various configurations planned for evaluation at HTHP conditions.

Activation

The initial series of low-temperature test runs (1 - 5, and 7) were attempts to activate P2 with the SPV exit nozzle in place. The general configuration for these runs was to place the SGD in its inactive mode at location B (over either a short stub of a cut-off candle filter element, or without any portion of a filter element underneath the SGD), while constraining the flow through locations A and C with either orifice plates and/or blanking plates mounted above the top of their respective filter elements. Attempts were then made to activate P2 by gradually increasing the flow into the SPV. By forcing enough of the system airflow through P2, the intent was to cause the lifting factor to exceed the threshold value needed to activate P2. For run 1, orifice plates with 0.75 inch diameter openings were placed over the candle filters at locations A and C. The SGD was placed at B over a short length of cut-off filter element. In this configuration it was not possible to force enough flow through P2 to induce activation. For run 2, orifice plates with smaller 0.375 inch diameter openings were placed at locations A and C. The maximum flow across P2 was increased by this change, as evidenced by an increase of the tubesheet ΔP from 7.7 to 16.8 in. H_2O at maximum SPV flow rate; however, there was still insufficient flow to induce P2 to activate. The lift factor calculated according to Equation 2 for the maximum flow rate achieved during run 2 was about 2300 kg/ms^2. For run 3, the orifice at location C was replaced by a blank plate, further increasing the flow through the SGD (the tubesheet ΔP at the maximum available system gas flow increased to 21 in. H_2O), but the lift factor achieved (2600 kg/ms^2) was still insufficient to activate P2. For run 4, the short length of filter element was removed from under the SGD, and the flow was increased to its maximum possible value. At these conditions, shown in Figure 14, P2 activated. The lift factor calculated for the last data recorded just before activation of P2 was 4100 kg/ms^2.

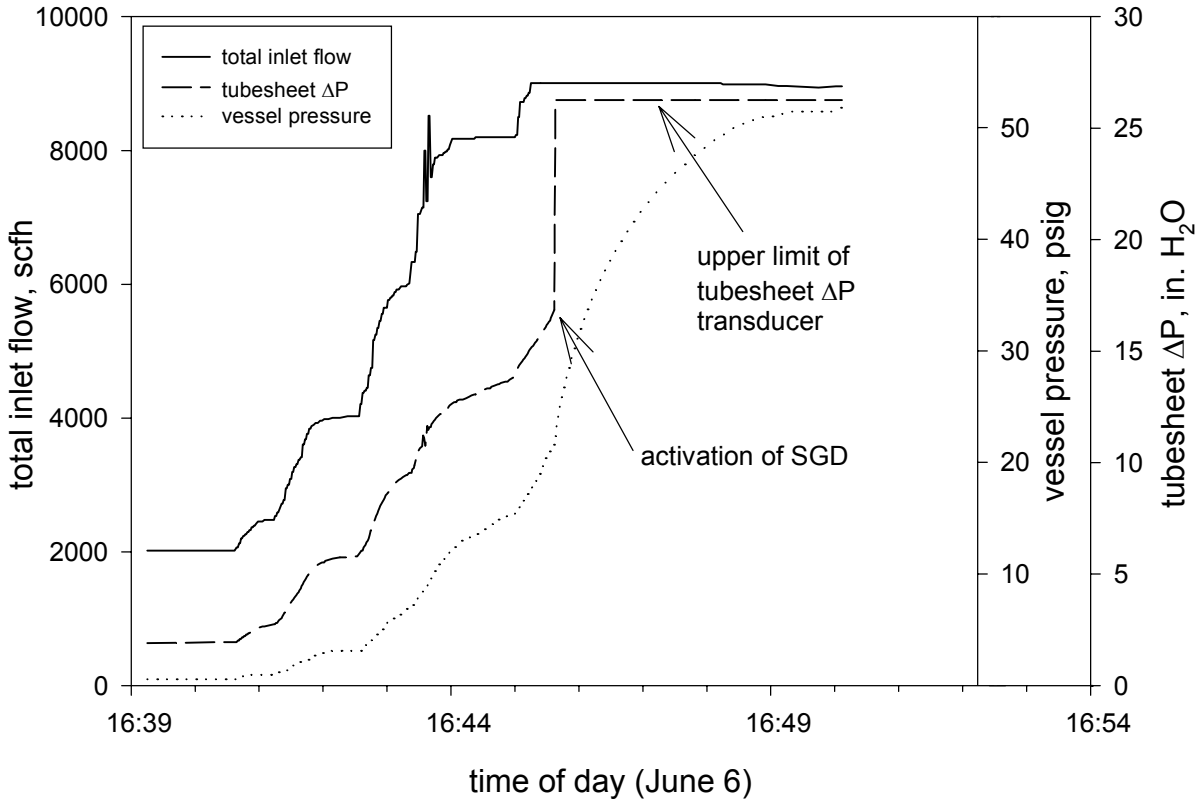

Figure 14. Activation of P2 during run 4.

The first four test runs conducted at the SPV illustrated that the DOE/NETL HTGSCTF would have to be operated at near its extreme upper limit of flow rate to activate P2 in this manner. Actual gas density and actual gas velocity in the SGD are combined in the lift factor ρv^2 that determines if the sealing plug will be lofted into its activated position at a given operating condition. Both gas density and gas velocity are in turn dependent on the temperature and pressure of the gas. In the first four SPV runs described above, the temperature of the gas was held at close to ambient levels, while the gas pressure in the SPV increased due to the back pressure relief valve located downstream of the SPV in the HTGSCTF system. Although any increase in gas pressure in the SPV causes a proportionate increase in gas density, it also causes a proportionate decrease in actual gas velocity. When these effects are combined in the calculation of the lift factor, the exponent 2 applied to the actual velocity term causes any increase in gas pressure (without any increase in gas temperature) to cause a proportionate decrease in the lift factor. Therefore, the first four runs performed in the SPV (and runs 5 and 7, which repeated the conditions set in run 4) presented the most challenging conditions for the HTGSCTF with respect to obtaining enough flow to activate P2. As noted above, flow into the SPV was limited to about 9000 scfh. (During some test runs the inlet flow may have exceeded 9000 scfh, but the HTGSCTF was unable to reliably meter and record flows any higher than this value.) Any decrease in the actual volume of this inlet gas due to pressurization by the back pressure relief valve further limited the lift factor available to the SGD.

As noted above, runs 5 and 7 were performed to reproduce the activation event that occurred in run 4. Each of these latter two runs apparently achieved total inlet flows (in terms of scfh) equal to the value at which P2 activated in run 4. However, because of the effects of pressurization of the SPV, the lift factors calculated for the maximum inlet flow rates during these two runs were lower than the value calculated for run 4. The maximum lift factor achieved in run 5 was 2600 kg/ms^2. The maximum lift factor in run 7 was 3900 kg/ms^2. Consequently, P2 did not activate during run 5 or run 7. (Apparently, in run 7 the SGD was operated just below the lift factor activation threshold of 4100 kg/ms^2 indicated by run 4.)

To characterize the activation of P2 without limiting the flow capability of the HTGSCTF caused by pressurization of the gas in the SPV, several test runs were performed without installing the exit nozzle at the top of the SPV. This limited any increase in the pressure of the gas in the SPV (above ambient levels) to the tubesheet pressure drop. In runs 9, 10, and 11 the SPV was operated in this manner, and the flow was manually increased in each run to induce P2 to activate. In each of these runs, the lift factor exceeded the threshold value of 4100 kg/ms^2 identified in run 4. P2 activated in runs 10 and 11 (see Figures 15 and 16); however, in run 9, the lift factor was calculated to have reached a value of 8400 kg/ms^2, but P2 did not activate. The reason P2 did not activate in run 9 is not known. Additional cold-flow characterizations including direct measurements of the flow through the SGD are recommended to resolve this apparent discrepancy with the calculation of the threshold value of the lift factor.

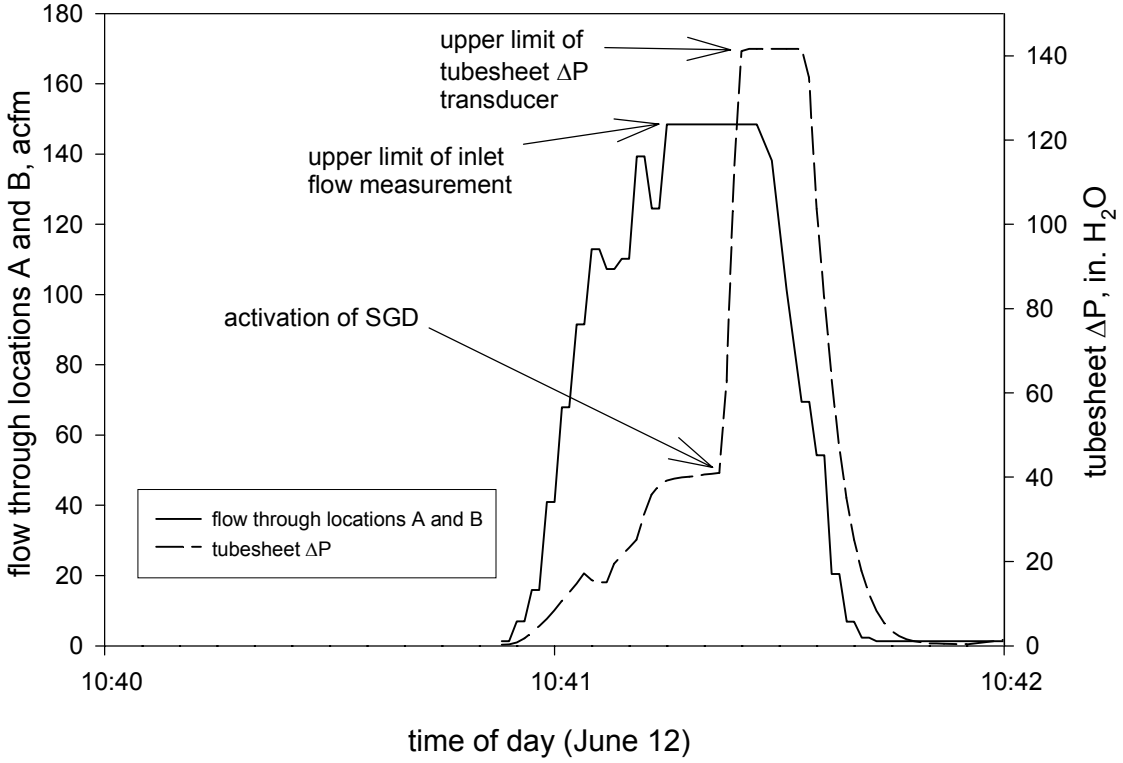

Figure 15. Activation of P2 by manually increasing flow (run 10).

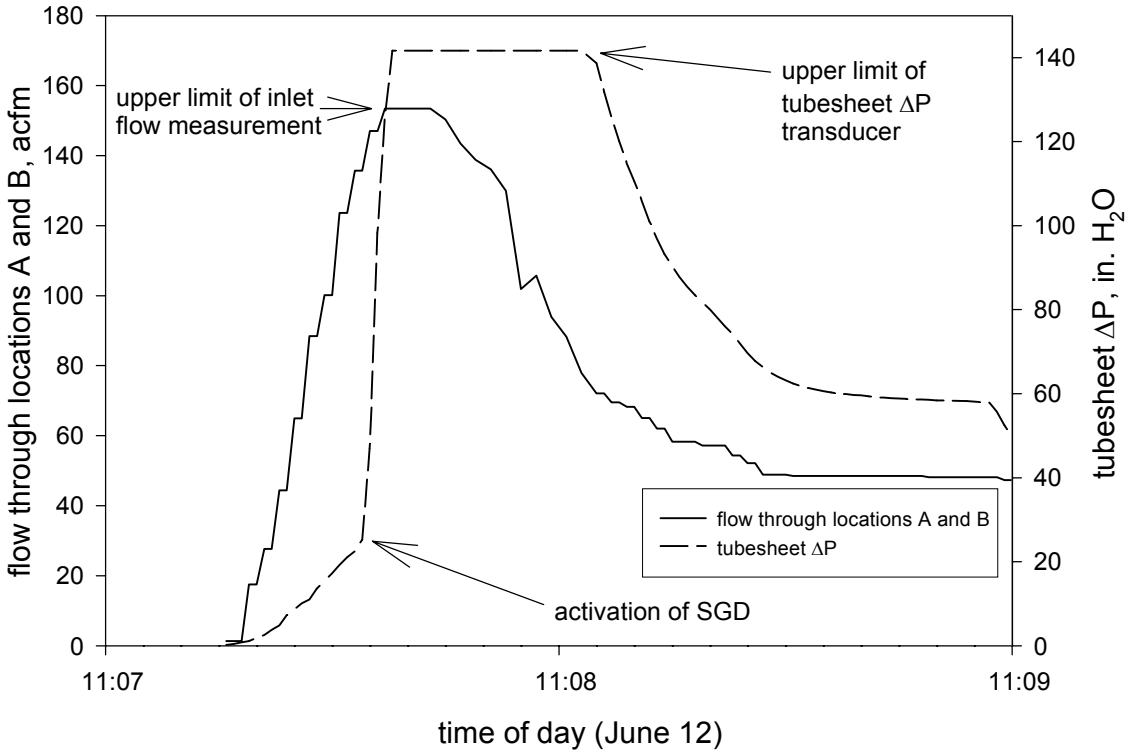

Figure 16. Activation of P2 by manually increasing flow (run 11).

Measurement of Flow/Pressure Drop Relationships

During several of the SPV runs, measurements were made to determine the pressure drop across the SGD as a function of the flow through it, as well as corresponding data for the 3/8" diameter orifice in place at location A during many of the test runs. Data obtained during run 6 showed that a flow of 37 acfm through location B on the tubesheet (without the SGD or any hardware or gaskets, etc.) generated a pressure drop of 2.3 in. H_2O. After the SGD activated in run 11, measurements of the pressure drop across the 3/8" diameter orifice were made as a function of the flow through it. These data are shown in Figure 17, and were used to estimate the flow distribution between the inactive SGD and the 3/8" diameter orifice for the calculations of the lift factor. For both conditions shown in Figure 17, the data indicate that about 20 % of the total flow passed through the 3/8" diameter orifice, while the remaining 80 % of the flow into the SPV passed through the cut-off candle and the SGD. Estimating the flow through the SGD is a key step in calculating the lift factor discussed above. This 80/20 flow split was used in the calculation of the lift factors for runs 3, 9, 10, and 11. A 95/5 flow split was used to calculate the lift factor for runs 4, 5, 7, and 14 (where the SGD was positioned over the tubesheet without a cut-off filter element underneath it). The data shown in Figure 18 were obtained in runs 12 and 13 to quantify the pressure drop associated with the cut-off filter element positioned at location B under the SGD for many of the test runs. Additional cold-flow measurements are recommended to further characterize the effects of flow restrictions and turbulence upstream of the FFMSGD on its operation.

Another effect that had to be taken into account to calculate the lift factor for several of the test runs was the rate of pressurization of the SPV at the point in time for which the flow through the tubesheet was being calculated. Because the flow measurement provided by the HTGSCTF system is obtained at the inlet to the system, any time the pressure in the SPV is increasing, the flow rate of gas entering the SPV is greater than the flow rate of gas passing through the tubesheet. Likewise, whenever the pressure in the SPV is decreasing, the flow across the tubesheet is greater than the flow into the SPV. This effect entered into the calculation of the lift factor for runs 4, 5, 7 in the ambient temperature tests, and runs 14 and 17 in the HTHP tests.

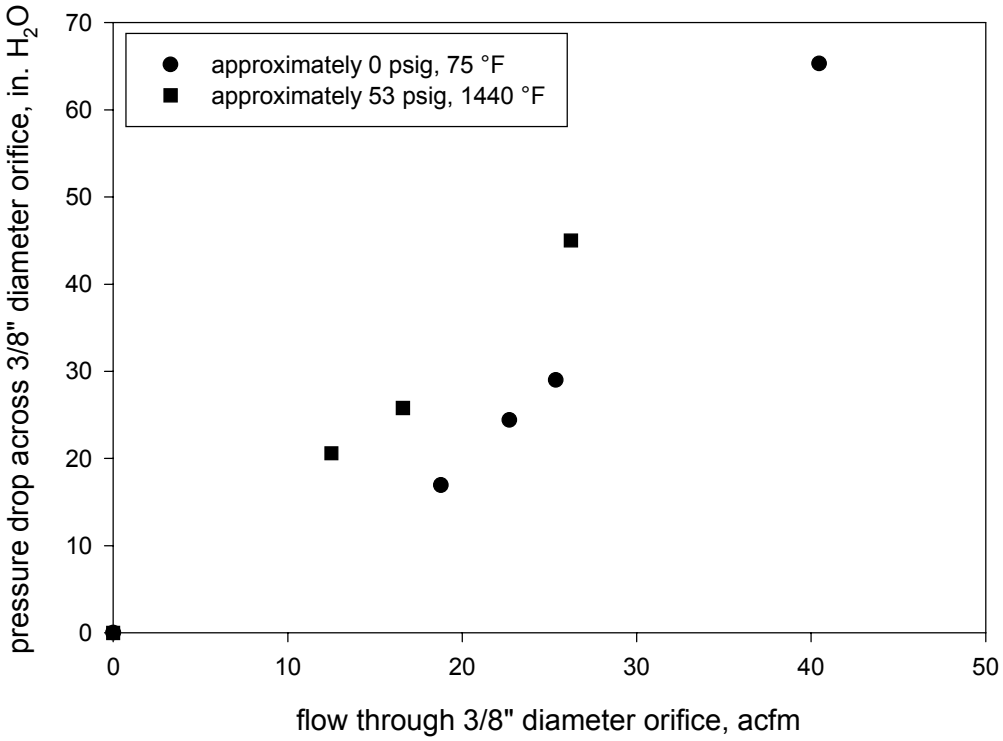

Figure 17. Characterization of the relationship between flow and pressure drop for the 3/8" diameter orifice at location A for ambient and HTHP conditions.

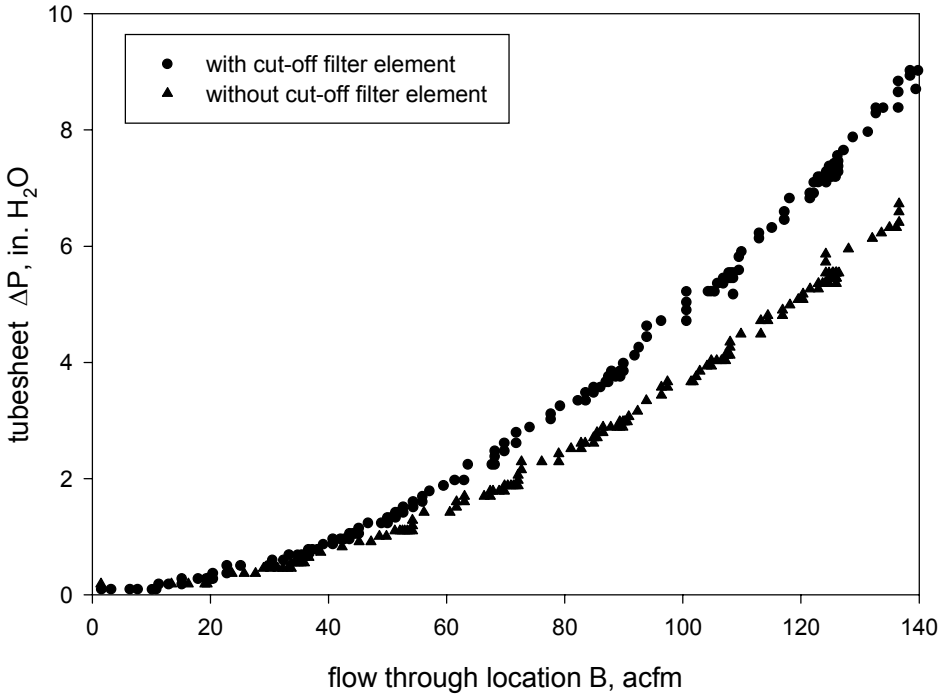

Figure 18. Pressure drop vs. the flow through location B at ambient conditions with and without a short section of cut-off candle installed beneath the tubesheet.

High Temperature, High Pressure Operation

The HTHP tests conducted at the HTGSCTF included activation tests much like those performed at ambient temperature, as well as tests of the ability of P2 to withstand reverse-gas pulses, and tests to determine the quality of the seal formed by the FFMSGD when activated at HTHP conditions. The primary changes in the operating characteristics of the FFMSGD at HTHP conditions result from changes in the density of the gas. The only other effect that operation at HTHP had on P2 resulted from differences in the coefficients of linear expansion for the 310 SS used to construct the majority of P2, and the Si_3N_4 from which the locking balls are formed. The coefficient of linear expansion of 310 SS is about 10×10^{-6} in./in./°F at around 1000 °K, while the corresponding value for Si_3N_4 is about 5.2×10^{-6} in./in./°F. This difference causes the locking balls to shrink in size relative to the rest of the FFMSGD when the device is heated. This may have caused the sealing plug to sit a little lower in the shell in its inactive position. (As discussed later in this report, this difference had no apparent effect on the ability of P2 to withstand reverse-gas pulses in the inactive mode.) The other result of this difference in expansion rates was evident in the post-test inspection of P2 after it had been activated at high temperature and then allowed to cool down to near ambient temperature for inspection and resetting. The fact that the locking balls had not increased in size as much as the rest of P2 had no effect on the movement and locking of the sealing plug in its activated position at high temperature. However, on cool-down, the locking balls grew relative to the rest of P2, causing them to be pinched between the body of the shell and the conical surface of the sealing plug. Because Si_3N_4 is harder that 310 SS, this effect caused slight indentations in the conical surface of the sealing plug where the balls were positioned when the device activated. The Si_3N_4 balls were not affected by being squeezed between the two 310 SS surfaces. Although these effects were observed in the HTHP tests, they had no measurable effect on the performance of P2. All these effects will be nonexistent when the locking balls are constructed out of 310 SS, which will become financially advantageous when a larger number of units are made.

Activation Induced by Manually Increasing Flow

The cold-flow tests performed in the SPV identified the role system pressure in the SPV had on achieving a sufficient lifting factor to activate P2. In the cold-flow tests, the HTGSCTF system was barely able to deliver enough flow through the SGD to activate it when the SPV was pressurized. For the tests conducted at HTHP conditions, the increase in gas temperature made it easier for the HTGSCTF system to provide sufficient flow to activate P2. In run 14, the temperature of the SPV was raised as high as possible, and the back pressure was held as low as the HTGSCTF system would permit, in order to maximize the lift factor available to P2. The sudden increase in the tubesheet pressure drop data presented in Figure 19 indicate a quick, complete activation of P2. The lift factor calculated for this activation event was 5800 kg/ms^2.

A qualitative post-test inspection of P2 showed that the device closed completely (Figure 20), and formed what appeared to be a total barrier to the passage of particles, and for all intents and purposes, an airtight seal as well. (A discussion of particle collection performance as indicated by the PCME is presented later in this report.) The activation of P2 during run 14 was followed by tests of the integrity of the activated device to withstand reverse-gas pulses (also discussed later in this report), as well as to prevent the passage of particles across the tubesheet.

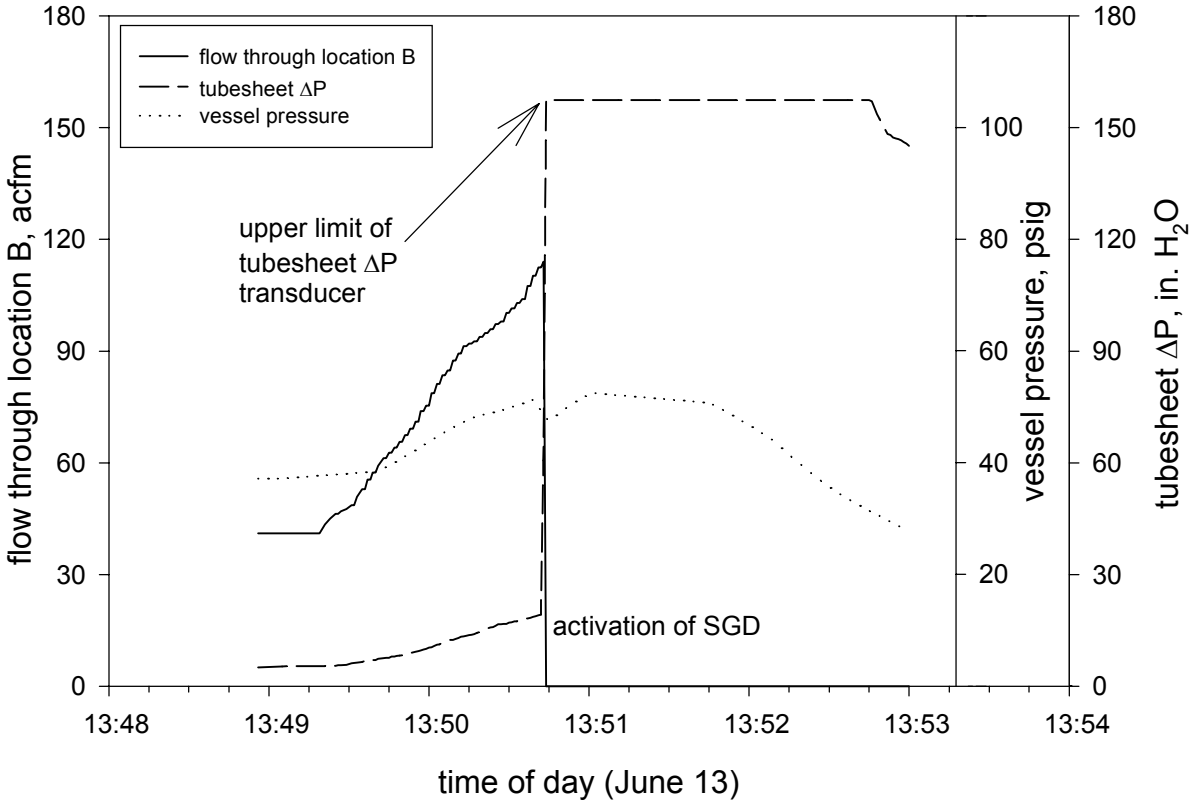

Figure 19. Data from run 14 showing the activation of P2 at 1547 °F. (The flow rate through location B shown on this figure has not been adjusted for the pressurization and depressurization of the SPV).

Figure 20. Top of P2 following run 15. A very small amount of ash and/or refractory material can be seen resting where the sealing plug meets the upper shell. The pulse tube is positioned over the top of P2.

Activation Induced by Filter Element Failure

Test run 17 on June 22 was set up to determine if the inactive SGD could withstand vigorous, repeated reverse-gas pulses in its inactive mode (discussed later in this report). Run 17 was also intended to compare the effectiveness of cleaning of a filter element fitted with P2 to the degree of cleaning experienced by another element operated in parallel without any SGD. (These data are also discussed later in this report.) However, after several hours (and eight 20-minute filtration and cleaning cycles) of HTHP testing in run 17, the filter element at location B (under P2) failed catastrophically, breaking completely off near the tubesheet, and falling into the SPV hopper. Although this unplanned event cut short run 17, it provided an excellent opportunity for the FFMSGD to activate following an on-line failure of its filter element. The failure was attributed to the thermal and/or mechanical force of the reverse gas pulse at location B. Immediately following the failure of the element at B, P2 activated, completely closing off the flow of gas through location B. Operation of the HTGSCTF continued through another three filtration and cleaning cycles, at which time the accumulation of tubesheet pressure drop reached system limits, and the system was shut down. A complete overview of the system vessel pressure, tubesheet pressure drop, and readings recorded by the PCME during run 17 is presented in Figure 21.

Examination of the data obtained by the Paragon TNT system and the PCME monitor provides a fairly detailed log of the specific events that occurred around the time the filter element at location B failed. The activation of P2 is apparent by noting the increased rate of accumulation of tubesheet pressure drop following the cleaning event that occurred at about 14:00. Because the flow through the SPV and the ash injection rate remained the same even after P2 activated, the face velocity through location A was doubled to 20 ft/min (location C was blanked off for run 17). The PCME also indicated a brief emission of ash at about 14:00, which is what would be expected if a small amount of particle-laden gas passed through the SGD as it was activating. The three subsequent peaks in the PCME readings at 14:20, 14:40, and 15:00 represent the resuspension and reentrainment of ash that passed through to the clean side of the tubesheet as P2 activated, but settled out on the various surfaces above the tubesheet. The agitation of this ash by subsequent reverse-gas pulses would cause some portion of it to be reentrained during each cleaning event, but the total amount reentrained would gradually diminish as the supply of ash that deposited above the tubesheet was depleted. The PCME data shown in Figure 21 agree with this sequence of events.

Detailed examination of the tubesheet pressure drop and vessel pressure data for several of the cleaning events during run 17 provide an even more precise identification of the sequence of events at the time of the element failure and the activation of P2. In Figure 22, the behavior of the system during one of the cleaning events (following the filtration cycle ending at 11:40) shows the typical reaction of the system to the cleaning procedures used. The cleaning pulse is derived by discharging the surge tank (pressurized to 350 psig) through a solenoid valve opened for 0.5 seconds. The first pulse in each of the cleaning events during run 17 was directed to location A (no SGD over the filter element). 20 seconds later (after the surge tank was fully recharged), a second pulse was directed to location B (over the top of P2).

In Figure 18 the tubesheet ΔP is lowered by pulsing location A, and further lowered by pulsing location B. Another effect that can be seen in the detailed examination of the tubesheet ΔP during the pulse cleaning events is the "bouncing" of the cleaning pulse wave back and forth across the tubesheet. This effect shows up in Figure 18 as the oscillations in tubesheet ΔP following the pulses at A and B.

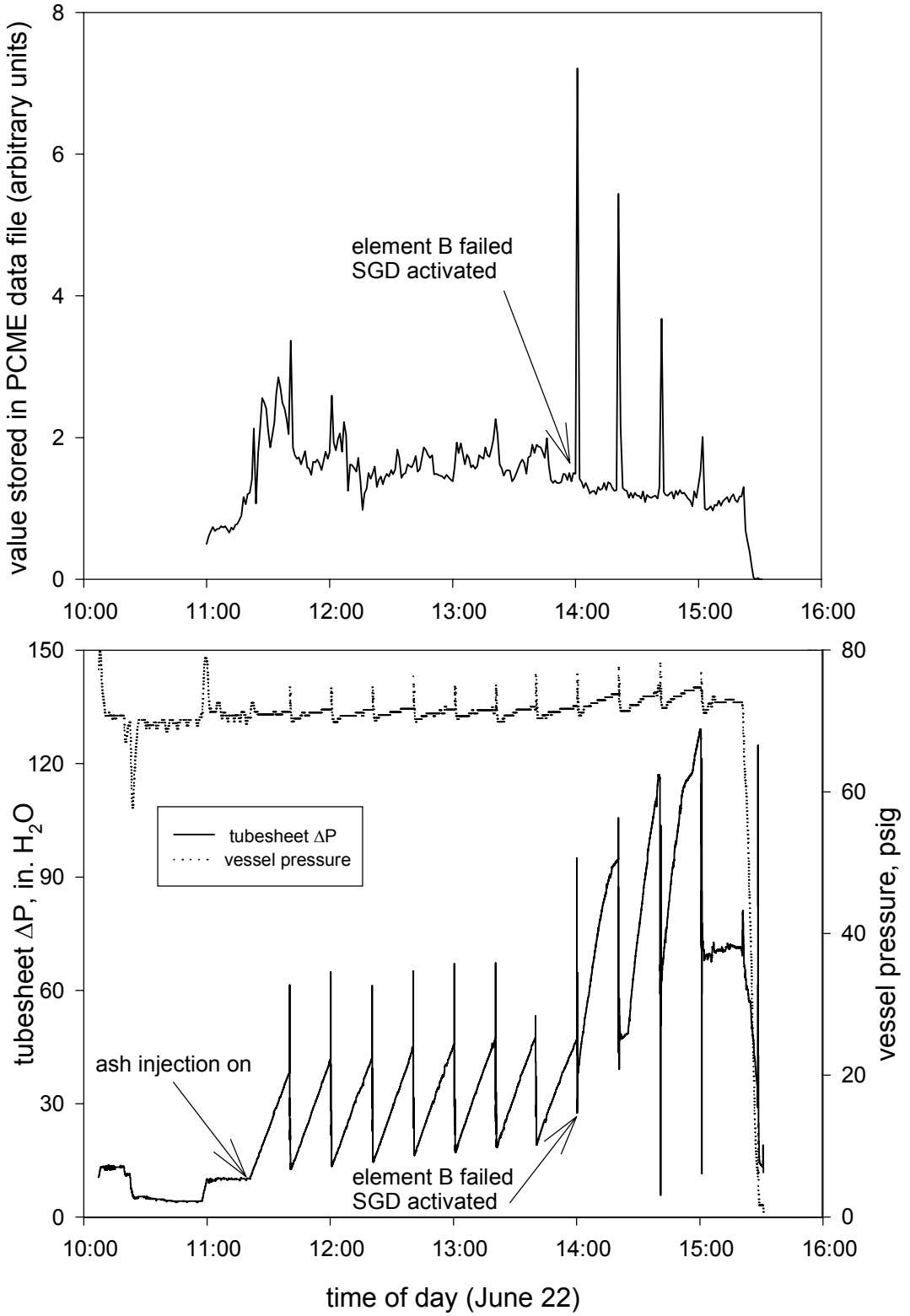

Figure 21. Summary of PCME readings, tubesheet pressure drop, and SPV pressure for run 17.

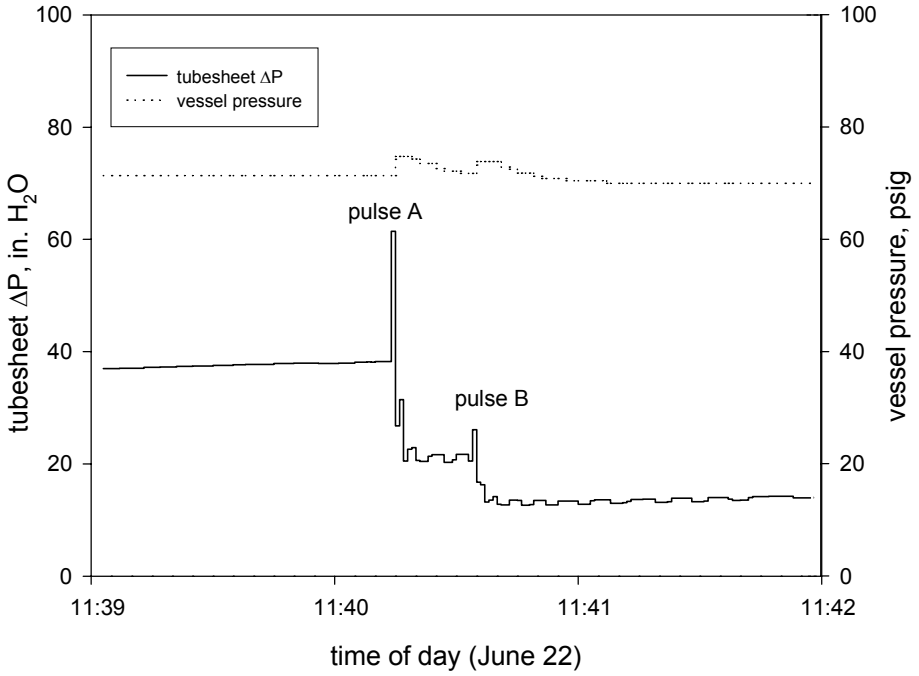

Figure 22. Detailed data for a pulse event prior to the failure of element at location B.

When the cleaning event that occurred at around 14:00 is examined in detail (Figure 23), a process of elimination can be used to determine when the filter element at B failed and when P2 activated. The tubesheet pressure drop is lowered by pulsing location A, but is increased after location B is pulsed. Therefore, at some point within a few seconds (at most) after the time the pulse was discharged at location B, the filter element at B has failed and P2 has activated. If the filter element at B had broken prior to the pulse at location B and P2 had not activated, the tubesheet pressure drop would have dropped to a very low value (less than 9 in. H_2O, based on data from run 14) because there would have been a very low resistance, nearly an open path across the tubesheet through the broken element at B. If the filter element at B had broken prior to the pulse at location B and P2 had activated, the tubesheet pressure drop would have been approximately 38 in. H_2O, the minimum value shown in Figure 18 for the period when it is known that P2 had activated. This analysis of the data has shown that the element at B was intact and P2 was inactive prior to the pulse at location B, and the element had failed and P2 had activated following the pulse at location B. Figure 24 presents a detailed record of the tubesheet pressure drop and SPV pressure for the next pulse event, which occurred at about 14:20. In Figure 24, it is apparent that the pulse at location B had no effect on the tubesheet pressure drop, other than the "bouncing" of the pressure wave noted earlier.

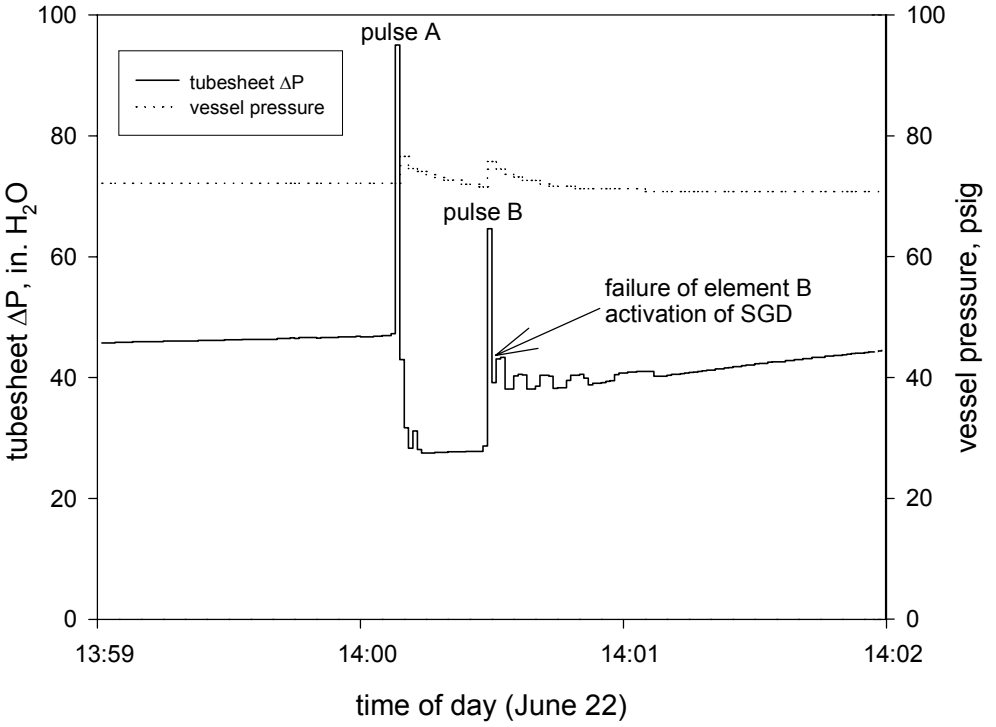

Figure 23. Detailed data for the pulse event that caused the failure of element at location B and the subsequent activation of P2.

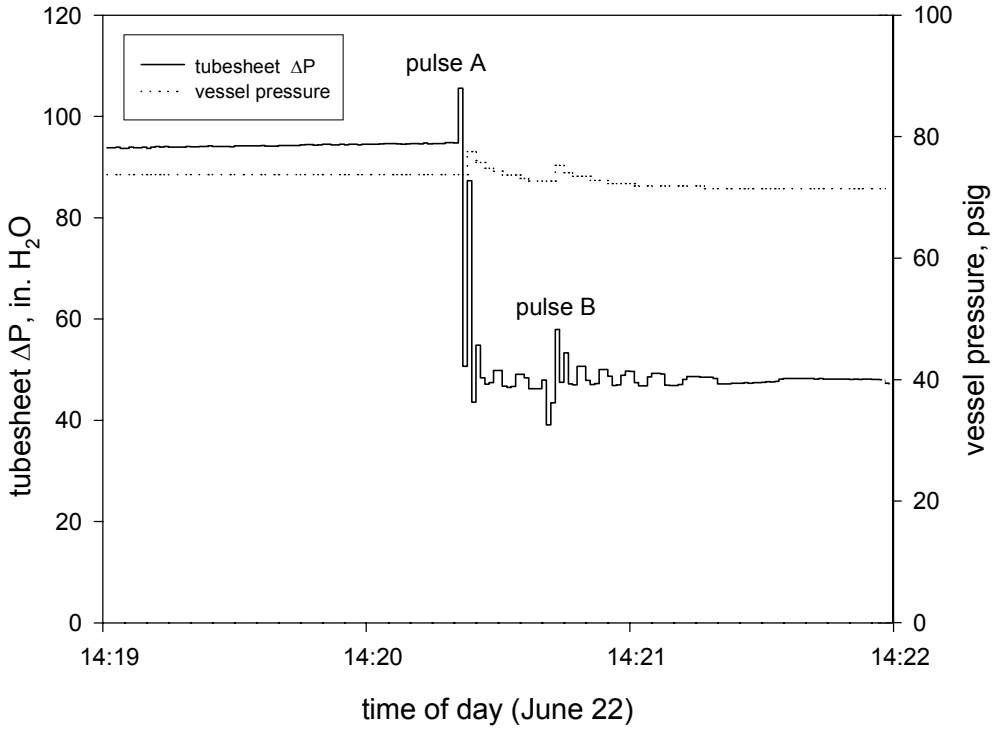

Figure 24. Detailed data for a pulse event following the activation of P2.

To compare the activation of P2 during run 17 with earlier activation events induced by manually increasing flow, it is useful to analyze the lift factors that were present at location B at various times during run 17 including some detailed examination of the lift factor around the time of the pulse at B that occurred at about 14:00:28. The first period that will be examined is a period of normal flow (in the middle of a representative filtration cycle prior to the failure of element B). At these conditions the flow through location B was about 30 acfm (a face velocity of 10 ft/min). For the SPV temperature of 1505 °F, and the SPV pressure of 71.3 psig, the lift factor at B is calculated to be 700 kg/ms^2, well below the threshold value for activation (estimated to be around 4000 kg/ms^2).

It is also useful to calculate the lift factor when location A is pulsed prior to the failure of element B. For this calculation, some estimates need to be made of the volume of pulse gas added to the vessel when the surge tank is discharged, as well as the movement of the pulse back up across the tubesheet after it enters the filter vessel. Pulse cleaning is performed on-line, meaning the tubesheet continues to experience a baseline flow across it of 60 acfm (two locations at 10 ft/min face velocity). When a pulse is discharged at location A, some volume of gas passes backward through the element at A, momentarily reversing the flow of gas through the element at A. Excluding the effect of the additional volume of gas introduced into the SPV by the pulse (discussed below), location B would momentarily take all 60 acfm of the flow across the tubesheet. This change would raise the lift factor at B to about 2800 kg/ms^2, still below the estimated activation threshold. To add in the effect of any extra flow through B derived from the volume of pulse gas that reached the dirty side of the tubesheet on the lift factor, it is necessary to examine the pressurization of the SPV achieved when location A was pulsed. On average, the pulses prior to the failure of element B caused the SPV pressure to increase by about 4 psig in one second or less. This increase in the internal pressure of the SPV equates to the introduction of 3.2 scf (or 2.2 acf at SPV conditions) into the SPV. Examination of the pressure decay in the SPV back to the baseline value of about 71.3 psig indicates that this excess volume of pulse gas exits the SPV through the tubesheet (locations A and/or B) in 14 to 15 seconds. Applying a simple algorithm to the passage of this extra gas volume back up across the tubesheet, it can be assumed that 25 % of this gas volume crosses the tubesheet in the first second, 25 % of the gas volume in the next two seconds, 25 % in the next four seconds, and the final 25 % is expended back up across the tubesheet in the next 8 seconds. It must also be assumed that the normal direction of gas flow through the element at A is rapidly reestablished following the momentary reversal of flow caused by the pulse at A.

Given these assumptions, it is possible to estimate the momentary flow rate through location B following the pulse at A. The maximum flow rate will occur when the first 25 % of the excess gas volume returns up across the tubesheet. The passage of this amount of gas across the tubesheet equates to a momentary flowrate of 33 acfm, which should distribute as no more than 17.5 acfm to B, and at least 17.5 acfm to location A. The total flow through B would then be about 47.5 acfm for the one second period following the reestablishment of normal flow direction through location A. This flowrate yields a lift factor of about 1750 kg/ms^2, which is well below the estimated activation threshold. As the rest of the pulse volume decays across the tubesheet, this factor will decrease even more, eventually returning to about 700 kg/ms^2.

Now it is necessary to examine the effect on the lift factor of the element at B failing. In the preceding argument, the decay of the pulse air volume across the tubesheet is divided between two candle locations. When location B was pulsed at about 14:00:28, the volume of pulse air entered the SPV, but the element at B is believed to have broken and fallen away from the tubesheet at the same instant. Because location B would then be a path of much lower resistance than the intact candle at location A, location B would take essentially all of the normal flow (perhaps 90 % of the 60 acfm) plus 90 % of the pulse air volume as it returned up across the tubesheet (90 % of 33 acfm). This would result in a momentary flow through B (for the first second following the resumption of normal flow direction through location B) of about 84 acfm. For this flow, the lift factor at B is calculated to be about 5450 $kg/m/s^2$, a value sufficient to activate P2.

Obviously, the discussion above contains a number of assumptions for flows and flow distributions that could not be directly measured in the SPV test runs. This discussion is intended to illustrate how the activation of P2 following the failure of its filter element can be considered to be consistent with the data obtained when P2 was activated by manually increasing the flow through it. More detailed measurements are recommended to understand the effects of the movement of pulse air volume through the FFMSGD.

Ability of the Inactive FFMSGD to Withstand Reverse-Gas Pulses

As noted above, one of the objectives of run 17 was to verify the ability of P2 to withstand repeated, vigorous reverse-gas pulses in its inactive mode. The data presented in Figure 21 clearly demonstrate that P2 remained in the inactive position through seven cleaning cycles. Although the test was planned to run for a total of 25 to 30 filtration cycles (it was stopped prematurely due to the filter element failure at B), the fact that P2 activated successfully after the failure of its filter element demonstrates that P2 was undisturbed by the seven vigorous cleaning pulses to which it was exposed prior to 14:00 on June 22.

Ability of the Activated FFMSGD to Withstand Reverse-Gas Pulses

Several of the SPV test runs exposed P2 in its activated condition to the vigorous reverse-gas cleaning pulses described earlier. In run 8, P2 was activated by manually lifting the sealing plug up and letting the locking balls roll into place prior to installing it on the tubesheet. Once HTHP conditions were established in the SPV, the top of the SGD was pulsed 15 times in a row (allowing enough time between pulses to fully repressurize the surge tank). Post-test inspection indicated that P2 remained in its fully activated configuration throughout this test. In run 15 (which was continued from run 14 in which P2 was activated at HTHP conditions by manually increasing the flow through it) P2 was again exposed to repeated reverse-gas pulses (24 in all). Post-test inspection following run 15 (Figure 16) indicated that P2 remained in its fully activated configuration throughout this test. A summary of run 15 is presented in Figure 21.

The integrity of P2 when exposed to reverse-gas pulses in its activated condition was also indicated at the end of run 17. Location B (and A) was pulsed at 14:20, 14:40, and 15:00 following the activation of P2 at 14:00:28. The photographs shown in Figures 26 and 27 show the top view of P2 following run 17. The sealing plug is securely in its activated position. The ash visible on the various surfaces shown in these figures may have been released across the tubesheet by the breakage of the filter element at B prior to the closure of the SGD; however, the element at A also broke at the end of run 17 (as noted by the system operator during the shut down procedures), and the subsequent opening across the tubesheet at location A during cool down of the SPV may have allowed a significant portion of the ash seen in Figures 26 and 27 to deposit above the tubesheet.

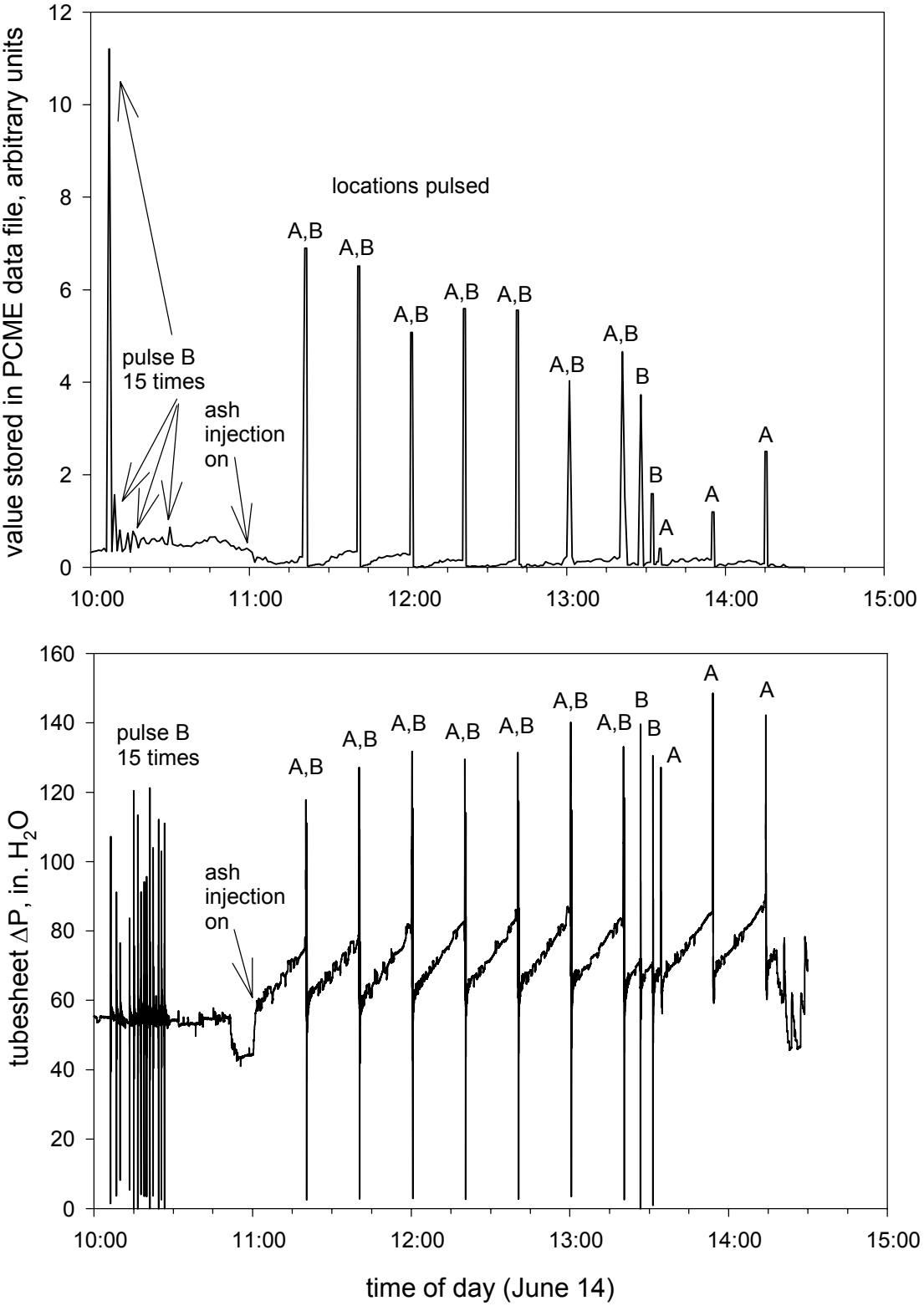

Figure 25. Summary of PCME readings and tubesheet pressure drop for run 15.

Figure 26. Condition of the region above the tubesheet following run 17.

Figure 27. Close up view of the top of P2 following run 17.

Effect of the Inactive FFMSGD on Pulse Cleaning

One of the objectives of run 17 was to compare the effectiveness of pulse cleaning of a filter element fitted with P2 to the degree of cleaning experienced by another element operated in parallel without any SGD. However, as discussed earlier in this report, after several hours (and eight 20-minute filtration and cleaning cycles) of HTHP testing in run 17, the filter element at location B (under P2) failed catastrophically, breaking off completely near the tubesheet, and falling into the SPV hopper. Considering the relatively open path through P2 in its inactive mode, this was probably the least crucial objective of the SPV testing. The SPV operators also indicated that to build significant ash cakes on the filters by collecting reentrained ash on the elements would probably take at least a week of operation. These reasons, and the fact that at the conclusion of run 17, DOE/NETL had no more filter elements in hand that could be used for testing caused the objective stated above to be abandoned. One way to determine the effect of P2 on pulse cleaning would be to perform cold-flow measurements in which the force of the pulse air coming through the outer diameter of the filtering surface of a candle filter element was measured with and without the FFMSGD in place.

Assessment of the Seal Provided by the Activated FFMSGD

Another major objective of the SPV tests was to determine the degree to which P2, once activated at HTHP conditions, provided a barrier to the transport of ash across the tubesheet. As noted in various discussions above, the appearance of P2 in its activated state as observed in post-test inspections conducted after runs 15 and 17 suggest that it provided a total barrier to entrained particles crossing the tubesheet. To supplement this circumstantial evidence of seal quality, several days of testing were conducted to obtain readings with the PCME device DOE/NETL provided and which was located in the outlet piping of the SPV system. The approach to obtaining this data was to compare baseline readings from the PCME prior to ash injection with readings following the initiation of ash injection (with P2 activated), and also to compare these data with PCME readings obtained on a different day for a configuration where, instead of P2 in its activated condition at location B, a blanking plate (simulating a perfectly activated mechanical failsafe) was installed at location B.

The PCME produces a data file which contains an average value for each minute of operation, although the display screen on the front of the PCME unit shows a value that is updated each second. Both the second-by-second values and the minute-by-minute averages are uncalibrated, and must therefore be used only as relative indications of entrained ash concentrations. The consistency of PCME readings from one day to the next had also not been verified prior to these SPV tests. An additional limitation of the PCME during these SPV tests is that it had not been interfaced with the Paragon TNT data acquisition system. Despite these limitations, data were obtained during runs 8, 15, 16, 17 and 18 which helped evaluate the quality of the seal formed by P2 during HTHP activation.

P2 was manually activated (the sealing plug was lifted into its activated position) at ambient temperatures and then installed on the SPV tubesheet prior to run 8. Therefore the PCME data obtained during run 8 may not be representative of the performance of P2 after activation at HTHP conditions. However, the PCME data obtained during run 8 are briefly discussed here. The data file normally created by the PCME was not available for the period of time covering run 8; however, manually recorded readings taken from the front panel of the PCME indicated that the baseline PCME reading was about 0.16 to 0.30. As indicated in Table 3, run 8 was performed without any injected ash. Therefore, if P2 was acting as a perfect barrier for the movement of entrained particles across the tubesheet in run 8, this PCME baseline value provides an indication of either the residual contamination of the region above the tubesheet with ash and/or refractory material, or a true baseline reading associated with an ash concentration of 0 ppm. More detailed PCME data were obtained during subsequent SPV test runs.

The effect of initiating ash injection on PCME readings was examined for runs 15, 16 and 18. (These comparisons are made for periods of time that should be unaffected by any prior reverse-gas pulses.) The PCME readings recorded in its internal data file indicate that the initiation of ash injection decreases the values stored by the PCME (for run 15 refer to Figure 25 at around 11:00, and for run 18 refer to Figure 28 at around 13:00). During run 15 on June 14, these readings ranged between 0.37 to 0.66 just prior to ash injection. Following the initiation of ash injection (at a nominal rate of 3 lb/hr, which was used for all periods of ash injection during these SPV evaluations), the PCME recorded values between 0.07 and 0.22. Similarly during run 18 on July 13, PCME data values prior to ash injection were between 0.12 and 0.23, while after ash injection was initiated the values ranged between 0.03 and 0.15. This same effect was observed during run 16, when the initiation of ash injection resulted in an immediate drop of about 60 % in the values recorded by the PCME in its internal data file. One possible explanation of why the PCME might generate lower values after the initiation of ash injection is that N_2 must be added for the ash injection system to function, which alters the gas composition reaching the PCME (as does pulse air). This altered gas composition may affect the responsiveness of the PCME. The fact that the PCME records lower values when ash injection is initiated suggests that the values it returns are subject, in a substantial manner, to factors other than ash concentration.

Despite the apparent sensitivity of the PCME to factors other than ash concentration, data obtained by the device were used to compare, in the presence of ash injection, the seal formed by P2 (activated at HTHP conditions - refer to run 15) to the seal formed by a blanking plate (refer to run 18). Run 15 was continued from run 14, in which P2 was activated at HTHP conditions by manually increasing the flow through it. The top portion of Figure 25 includes data recorded by the PCME's internally stored data file for all of run 15. These data show that the PCME was responsive to a series of reverse-gas pulse events. The data also suggest a baseline level of PCME readings (between pulses) of around 0.03 to 0.33.

The peak values recorded by the PCME corresponding to pulsing location B (where P2 was located) were around 3.7 to 6.9. The appearance of P2 following run 15 (Figure 20) suggests that these peaks represent ash particles and/or ceramic insulation particles reentrained from various surfaces in the region above the tubesheet by the force of the reverse-gas pulse. It is logical to assume that the pulses discharged at location B would cause sufficient agitation in the region above the tubesheet to dislodge and reentrain some of these particles. As noted above, the pulse used was the maximum pressure available to the SPV system, and was discharged directly above the top of the top of the SGD, which was fully closed. Therefore the volume of gas discharged at location B would be deflected with significant force directly against other surfaces above the tubesheet.

The objective of run 18 was to reproduce the activities and measurements of run 15, with the exception being that instead of the activated SGD being placed at location B, a blank plate was placed at this location. When the PCME data recorded in its internal file during run 18 are examined, the peaks associated with the reverse-gas cleaning sequences are significantly lower (0.12 to 0.15) than the corresponding values recorded during run 15. The data the PCME recorded from run 18 suggest a baseline level of PCME readings (between pulses) of around 0.01 to 0.02.

The PCME data from run 18 (with the blanking plate) seem to indicate that the particle concentration (both between pulses and during pulse events) is somewhat diminished in comparison to run 15 (with P2 activated). However, there are no calibration data available which convert these differences to known particle concentrations. The lack of calibration of the PCME signal for the conditions of these SPV tests precludes the conversion of these outlet measurements to a standard basis, such as ppm. The differences between the run 15 PCME data and the run 18 PCME data may not be significant in terms of ppm. In fact, the baseline PCME values for runs 15 and 18 are less than values measured prior to ash injection. Therefore it is certainly possible that the baseline emissions during run 15 and run 18 are both well below 1 ppm.

During post-test inspection after the conclusion of run 16, which was performed in an attempt to get baseline PCME values associated with a "perfectly" activated SGD (a blank plate), it was discovered that the filter element at location A had partially failed. Long cracks (about 0.8 m) were apparent on two sides of its length. The PCME outlet emissions monitor data showed a baseline value of about 1.1 between reverse-gas cleaning pulses, and values corresponding to the pulses of about 12 to 24. It is reasonable to assume that these values, which were higher than either the run 15 or run 18 data, reflect the existence of the cracks identified in the element at location A.

Examination of the data recorded by the PCME during run 17 also provide some indication of the consistency of the PCME readings between comparable run conditions on different days. Prior to the filter element failure at location B at about 14:00, the baseline PCME reading was about 1.7 (refer to Figure 21). After the element failed and the SGD activated, the PCME readings between back pulse events declined slightly to around 1.1. Also, the PCME baseline value of around 1.7 prior to the failure of the element at B is significantly greater than the baseline values from either run 15 (about 0.2), or run 18 (about 0.02). The most likely explanation for this difference was that either the region above the tubesheet was much more contaminated at the start of run 17 than it was prior to run 15 or run 18, or that the PCME reading can vary significantly from day-to-day for comparable conditions.

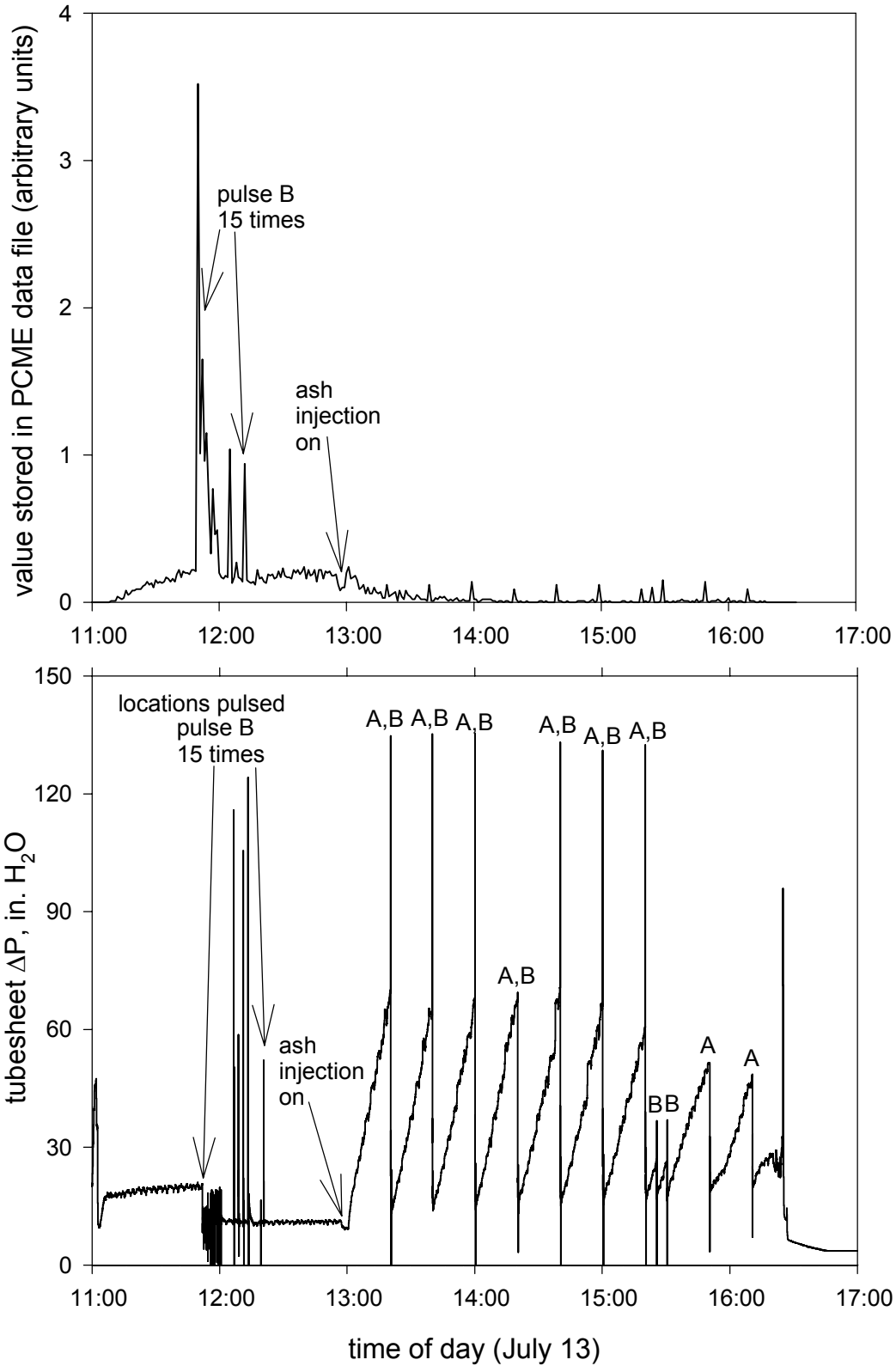

Figure 28. Summary of PCME readings and tubesheet pressure drop for run 18.

In addition to the factors related to absolute sensitivity of the PCME, the fact that run 15 and run 18 were made about four weeks apart may make the comparison of the absolute levels of the PCME values between these two runs much less meaningful. Another key difference between these runs may have been the degree to which the region above the tubesheet was free of ash deposits. Although reasonable efforts were made prior to each of these runs to ensure that the region over the tubesheet was clean, a small ash deposit remaining above the tubesheet prior to the run, or formed during the run, may have caused the minor differences between the PCME readings recorded for these two runs. In fact, after run 15, a small deposit of ash was located on the outside of the shell of the SGD (Figure 29). The location and appearance of this deposit seem to indicate that it was formed by ash leaking from the filter location (A) next to the SGD, and not from any leak associated with the SGD itself. (The ash deposit on the outside of the shell can also be seen in Figure 30, adjacent to the hold-down plate at location A. Location A is located clockwise of the SGD, in the lower right of the tubesheet area.)

Figure 29. Condition of the SGD after run 15. The small ash deposit visible on the outside of the shell near the bottom of the SGD may provided a source of ash particles that could have been reentrained by the reverse-gas cleaning pulses.

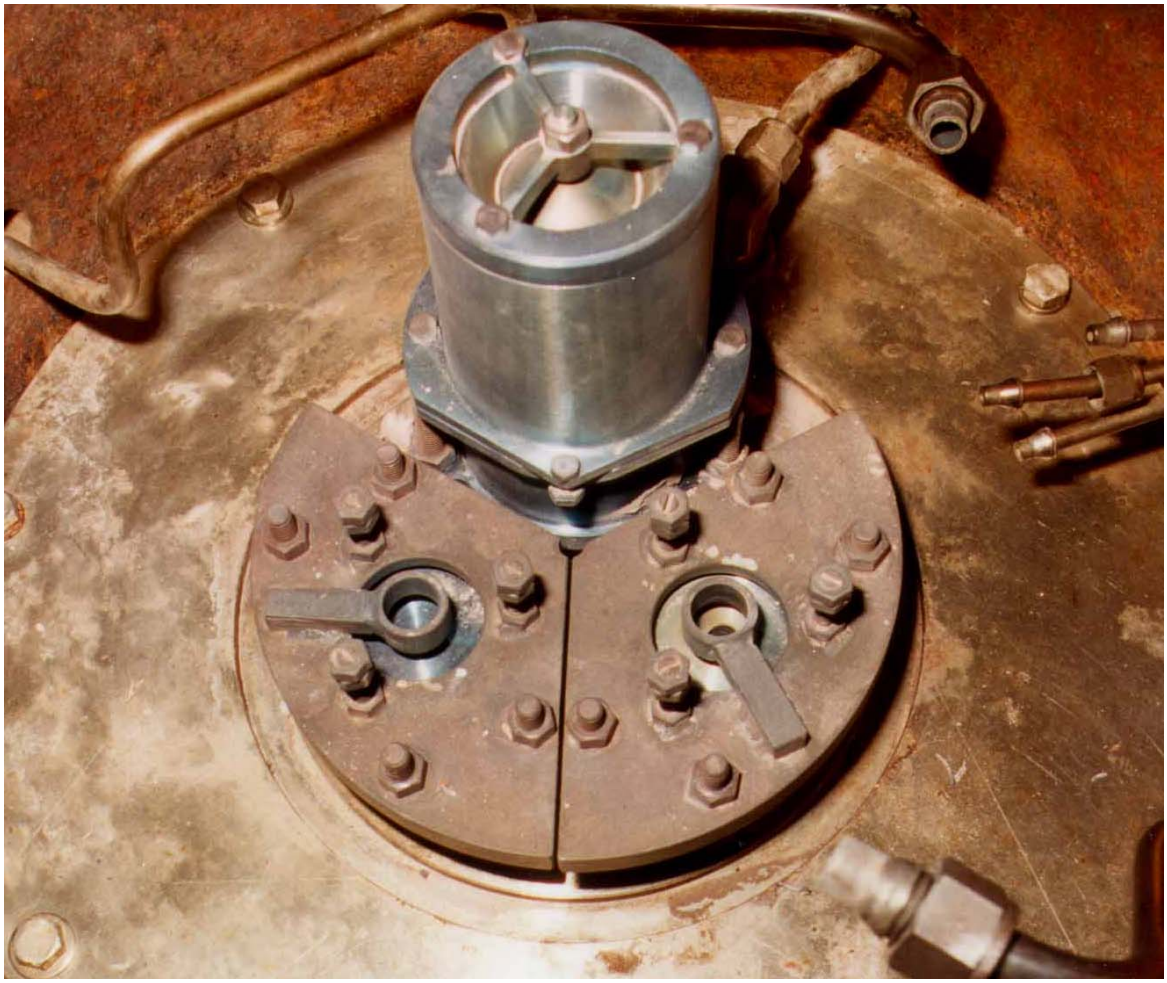

Figure 30. Condition of the SGD and the tubesheet following run 15. The small ash deposit on the outside of the SGD shell can just be seen behind the stud extending up from the hold-down plate at location A (clockwise from the SGD).

Detailed Examination of PCME Performance

To assess the performance of P2 using the PCME data, it is necessary to interpret the value the PCME records in its internal data file. As noted above, the PCME produces a data file which contains an average value for each minute of operation. When the concentration of suspended particles is relatively constant, the differences between the information provided by data on the PCME display screen (updated each second) and the trend indicated by the average values stored by the PCME each minute are similar. However, when the signal representing the concentration of ash is changing rapidly, as in the period of time following a reverse-gas cleaning pulse, the second-by-second data displayed on the PCME screen provides what appears to be important detailed information that is not recorded by the device in its internal data file (containing the minute-by-minute averages).

During several of the pulse events conducted during run 15, the data displayed on the PCME screen were manually recorded at 20 second intervals. In Figure 31, data manually read off the PCME screen at 20-second intervals are compared with data recorded by the PCME for the same periods of time. Although these data are similar for most of the time, the values in the data file repeatedly drop well below the values displayed by the screen in the periods of time immediately following the reverse-gas pulses (which correspond to the large vertical spikes in the data shown in Figure 31).

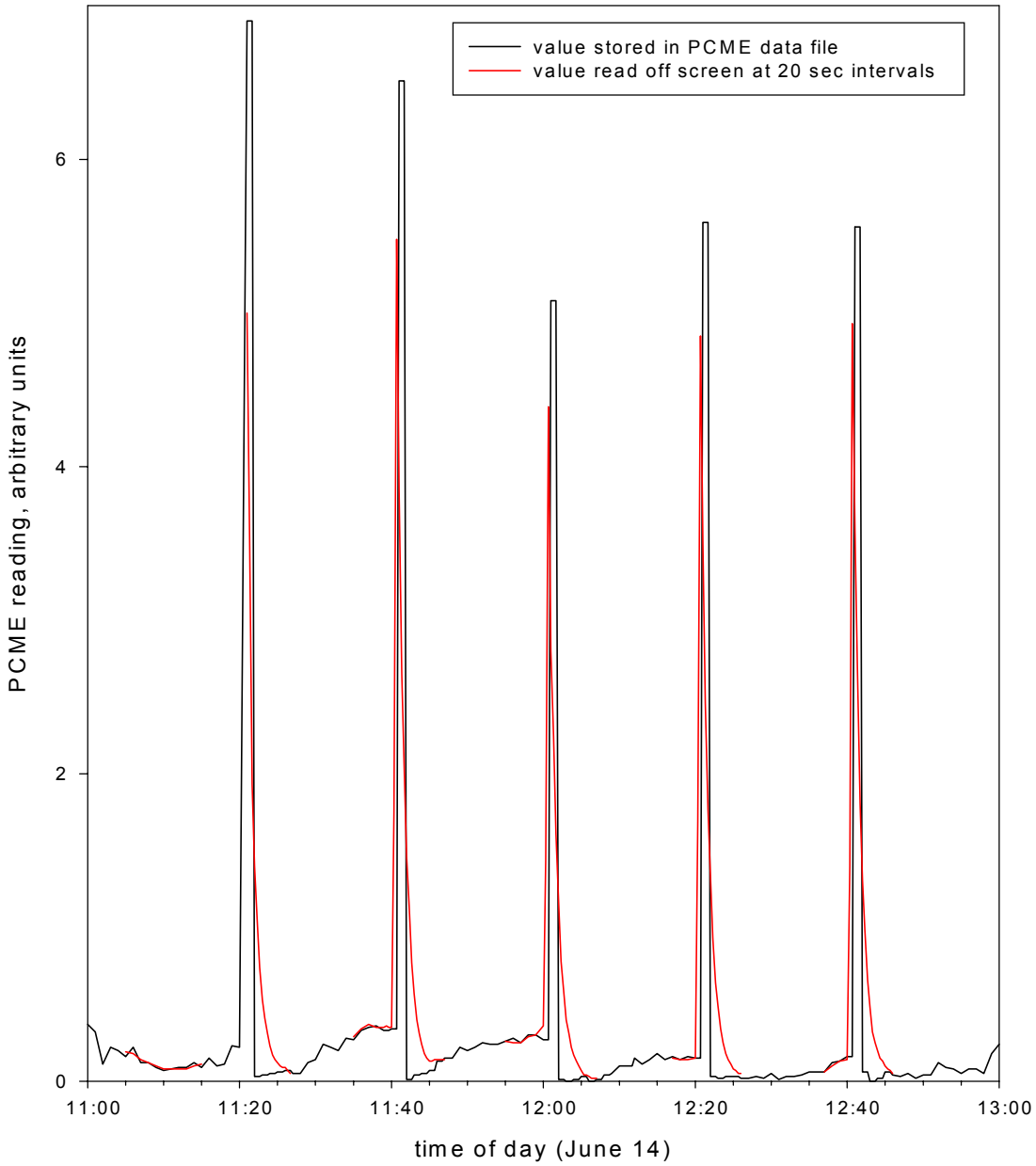

Figure 31. Readings from the PCME data file compared with values read off the PCME display screen at 20 second intervals for selected time periods during run 15.

During run 18, a video camera was used to record the screen display of the PCME so that second-by-second values obtained by the device could be examined in detail, and compared with the minute-by-minute values the PCME recorded internally. The PCME seemed to respond quickly to the pulse cleaning events during run 18 (four of which are examined in detail in Figure 32). For each of these four pulse cleaning events, the PCME was able to observe the effect of pulsing location A separately from location B, which was pulsed about 20 seconds after location B. The relative heights of the location A (normally configured candle filter element) pulse cleaning spike and the location B (blank plate) seems to indicate the effect of the reflection of the volume of pulse air off the blanking plate and the subsequent effect this agitation of the air above the tubesheet has on the reentrainment of particles. For each of the four events shown in Figure 32, the value recorded by the PCME for the minute corresponding to the pulse event was essentially the average of the 60 readings displayed by the device during that minute. The PCME internally recorded values about 0.09 to 0.14 for these four pulse events.

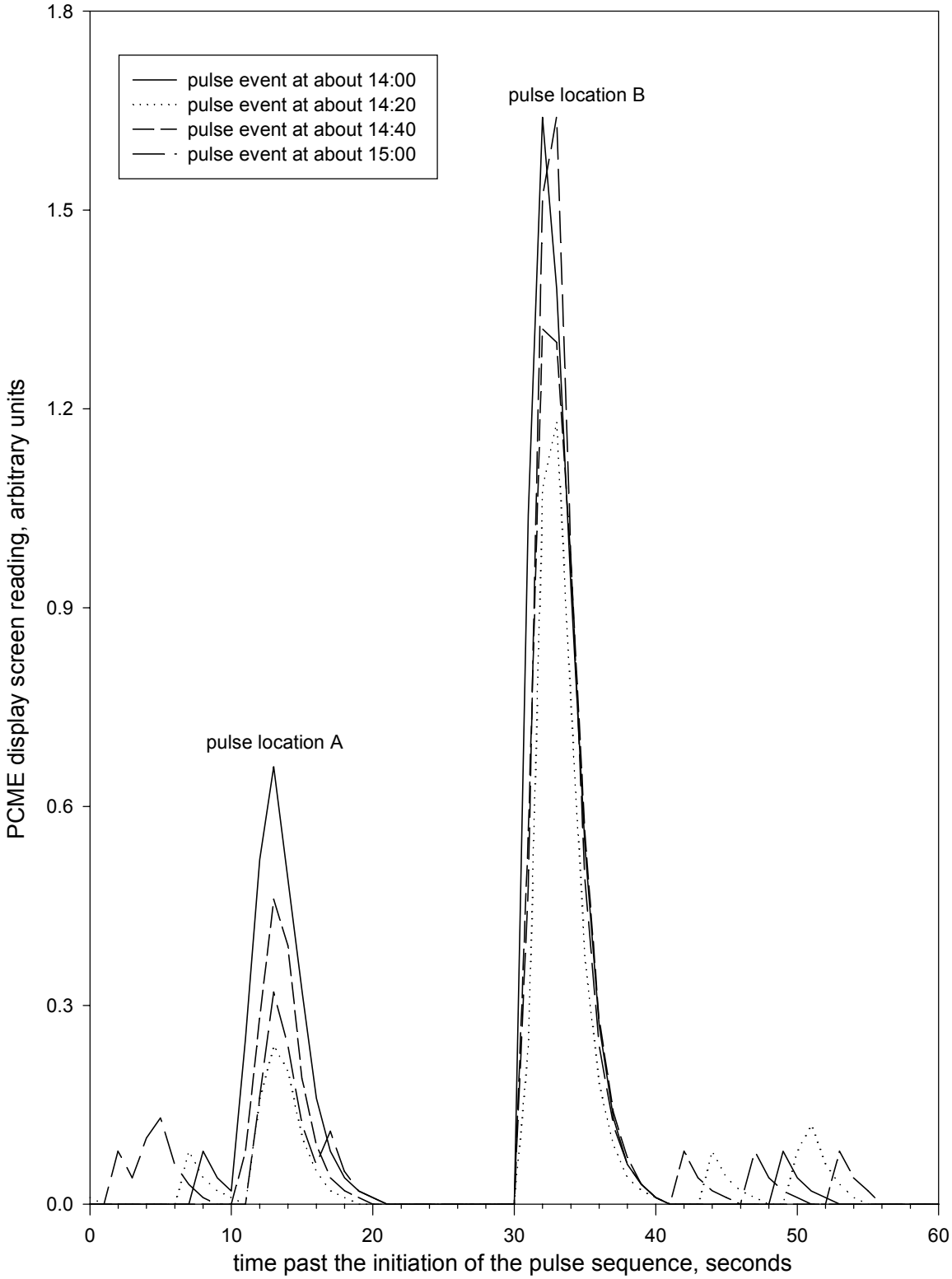

Figure 32. Reading displayed on the PCME screen through four separate pulse events during run 18.

PILOT-SCALE FFMSGD TESTING AT THE PSDF

The final step planned for this project is the evaluation of the FFMSGD concept during one of the periodic PSDF HTHP test runs. The first opportunity for this evaluation was in late 2001, although PSDF system delays moved the evaluation to February or March 2002. A third FFMSGD prototype, P3, was designed and constructed especially for this PSDF evaluation. The staff of the PSDF provided information relating to the expected operating conditions, as well as requirements for external dimensions and materials. Because of delays in the PSDF test schedule, the final results of the evaluation are not included in this report.

DEVELOPMENT OF A DESIGN NOMOGRAPH

One of the most important steps in the ultimate application of the FFMSGD technology to an HGCU filter is the proper selection of the activation threshold of the individual FFMSGD units. The range of operating conditions that might be expected at the HGCU filter, as well as the likely filter element failure scenarios, should be taken into account during the design phase. Figure 33 illustrates the conditions under which the FFMSGD would activate in the event of a isolated filter element failure in a conventional HGCU filter. (The values for the various quantities noted in Figure 33 are generally related to the values measured for P2. However, the relationships between the quantities and the operating parameters of the HGCU filter shown in Figure 33 can be generally extrapolated to all FFMSGD designs.) A sufficiently high upward force, generated by the dissipation of pressure across the annular orifice, must be applied to the sealing plug to initiate activation of the FFMSGD. As Equation 1 defines, this force is proportional to the density of the gas and the square of its velocity through the annular orifice described above. The weight of the sealing plug and the cross-sectional area of the annular orifice between the plug and the shell can be adjusted in the design process to set this threshold of activation at the desired level. Identifying the proper activation threshold requires some knowledge or estimate of the operating conditions at the point in the process where the FFMSGD will be located (usually the filter tubesheet). Proper selection of the activation threshold will ensure that the only condition sufficient to activate the device will occur when its filter element fails. In Figure 33, the activation threshold (7 in. H_2O) is about five times the normal pressure drop across the annular orifice (1.5 in. H_2O), and almost three times the maximum foreseeable value for the process. (This maximum value is roughly based on operation at an HGCU filter when its most extreme and abnormally high filtering velocity was momentarily experienced.) By setting this threshold above the maximum foreseeable value for the intended process, a safety margin against unintended activation, as identified in Figure 33, is established. In the case of the failure of its filter element, the magnitude of the pressure differential across the tubesheet determines the gas velocity through the SGD. Therefore, as the threshold of activation is increased, the minimum tubesheet pressure drop at the time of filter element failure, below which the FFMSGD will not activate, is also increased (see Figure 33). The relationships governing the activation of the FFMSGD allow a wide “window of activation”. However, balancing the insensitivity to process upsets with the ability to activate with a low tubesheet pressure drop

must involve the process operators in the FFMSGD design. As the magnitude of the normally expected pressure drop across the filter element at risk of failure increases, a much wider latitude can be exercised in setting the limits of the FFMSGD's window of activation. Also, as the margin of safety against unintended activation is decreased in the design phase, there is an improved ability of the FFMSGD to activate in the presence of filter element failures that are less severe than a total breakage of the element. Total catastrophic failures of filter elements have generally been the rule at pilot-scale HGCU filters; however, there may be future applications or designs in which these less severe element failures become a threat.

As part of the process used to select the proper activation threshold, plug weight, and annular orifice dimensions for P3, a design nomograph was developed in Microsoft® Excel. The nomograph allows the designer to select the safety margin against unintended activation (as described above), while optimizing the ability of the FFMSGD to activate in response to a filter element failure. The nomograph takes process operational data or estimates and combines them with the desired safety margin to calculate the physical dimensions of the FFMSGD annular orifice and the design weight of the sealing plug.

FFMSGD DESIGN FOR PSDF TESTING

In order to maximize the useful results from the development and testing of a third prototype FFMSGD, it was decided to investigate an alternate sealing technique in the design of P3. The basic design used for P3 is shown with some details obscured in Figure 34 (but completely detailed in the companion appendix to this report). Although there were some changes to the internal dimensions of P3 compared with the earlier prototypes, the principle of activation remained the same. The only significant change was from a metal-to-metal spherical seal to an alternative design, which is fully discussed in the companion appendix. This design of P3 may allow the FFMSGD technology to be applied to a wider variety of processes than might be possible with only the metal-to-metal seal design.

Like P2, P3 was fabricated from 310 SS, and included Si_3N_4 locking balls. The two halves of the shell were joined near the bottom of the body of P3 with bolts and nuts torqued according to specifications provided by the PSDF staff. These specifications allowed the ceramic woven fiber gasket shown in Figure 34 to provide a seal against particles bypassing the filter element.

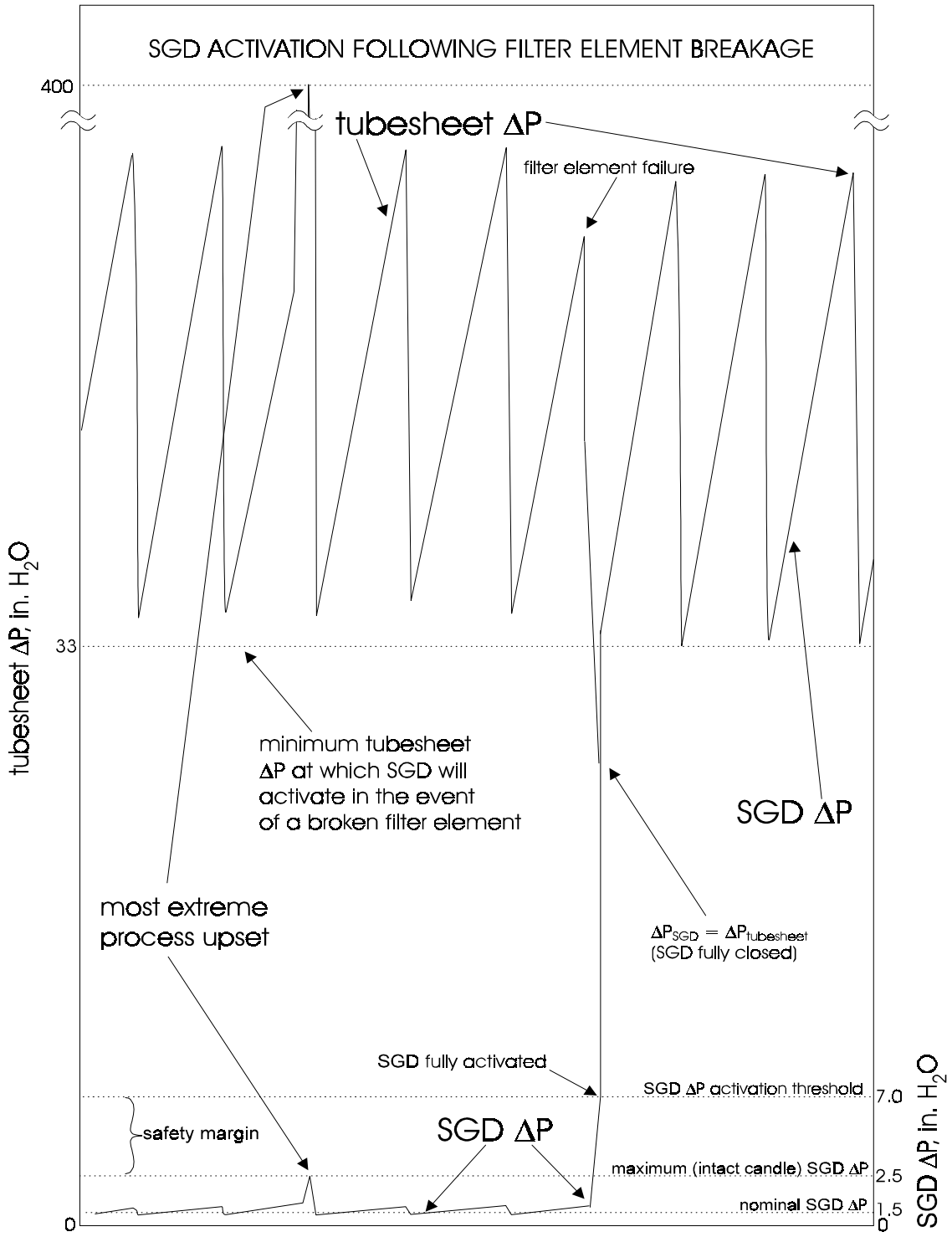

Figure 33. Idealized relationships between the pressure drops across the tubesheet and an SGD before, during, and after the failure of a filter element and the resultant activation of its SGD.

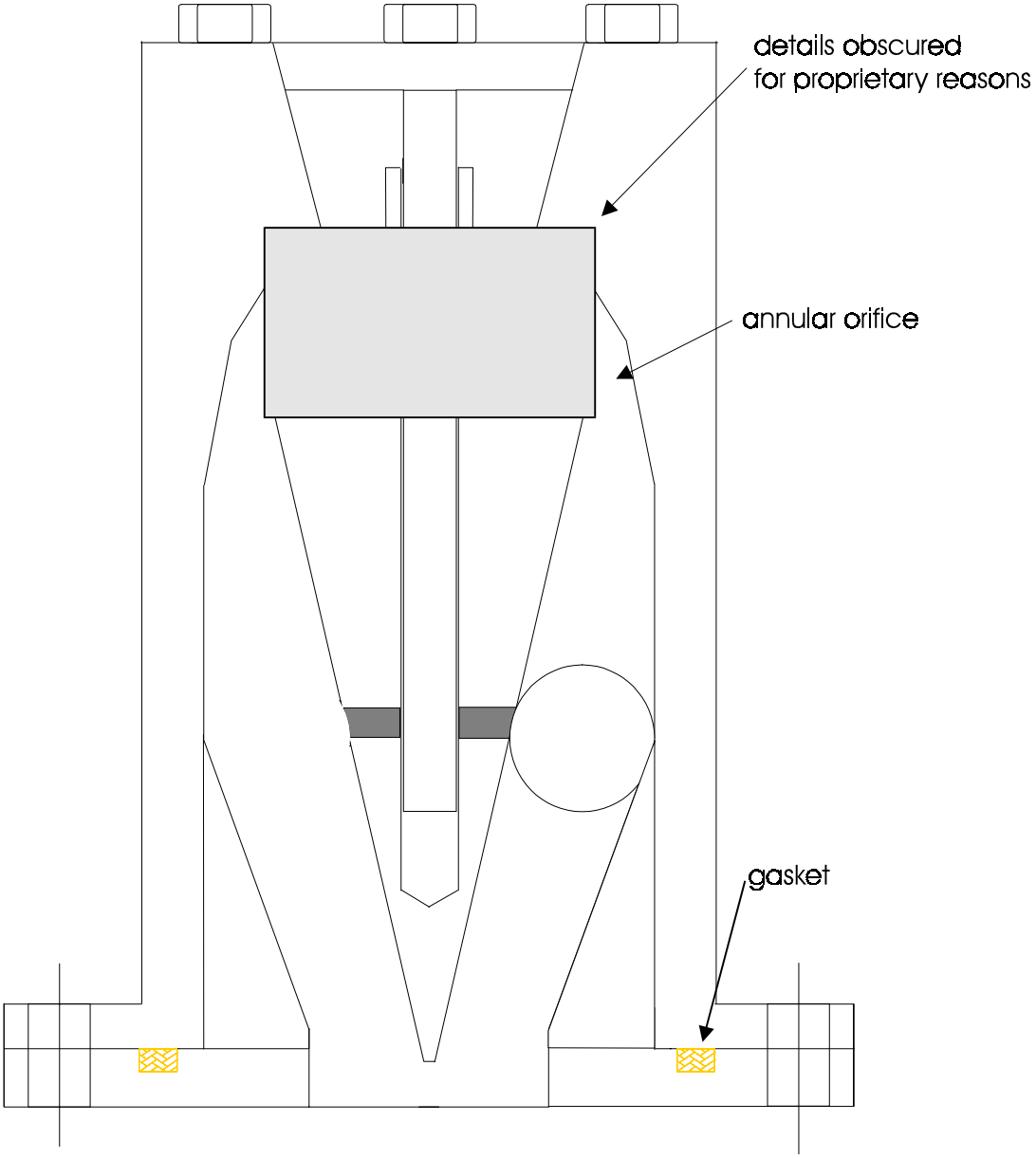

Figure 34. Basic design of the FFMSGD prototype P3 in its inactive position. (Details of the sealing design have been obscured.)

TEST OBJECTIVES

Because over 90 filter elements are normally located in parallel on the HGCU filter tubesheet at the PSDF, this pilot-scale test of P3 was not designed to assess the quality of the seal formed during activation, but rather to determine if P3 would remain inactive during most of the PSDF test, and then if it could subsequently be induced to activate at typical operating conditions following this extended exposure to the HTHP environment. The sealing approach used for P3 in the PSDF tests will provide the means of sensing whether P3 has activated.

TEST PLAN

The objectives of the PSDF evaluation of P3 require the condition of P3 (inactive vs. activated) to be constantly monitored throughout the PSDF test run. To achieve this objective, the porous metal filter element below P3 was specially modified as shown in Figure 35 to include a pressure line leading from inside the filter element (on its clean side, but below P3) to the outside of the filter vessel. By reading the pressure difference between this line and the existing pressure line that the PSDF uses to sense the pressure above the tubesheet, it is possible to determine whether P3 has activated. When P3 is in its inactive condition, this pressure differential is the pressure lost (estimated to be about 2 to 3 in. H_2O) as the filtered flue gas passes through P3 and the additional failsafe unit (discussed below) that the PSDF staff placed above it. Because the PSDF staff also wanted some protection in case the filter element under P3 failed and P3 did not activate, a second failsafe with a pore-plugging design was installed above P3. Although this setup does not mimic the ultimate configuration that is envisioned for the FFMSGD, it should not interfere with the objectives of this test. If P3 activates, the pressure drop across it (and the second failsafe above it) will be essentially equal to the pressure drop across the tubesheet (probably well in excess of 50 in. H_2O). The expected sudden change of this measured pressure differential to this higher value will be the indication that P3 has activated.

As with the tests of P2 at the DOE test facility, inducing the failure of the filter element below P3 is not an option for the pilot-scale test at the PSDF. Therefore, the filter element was also modified to include a second line from inside the element to outside the filter vessel. This second line was installed to allow a large volume of nitrogen to be discharged from a compressed gas cylinder into the inside of the filter element in order to attempt to activate P3 on command. By discharging a sufficient flow of nitrogen up into the filter element, it is expected that enough flow will move through P3 (rather than backwards across the body of the candle and back through the filter cake) to activate it. Because it will not be possible to determine the relative distribution of the flow discharged from the nitrogen source, the amount of nitrogen delivered from the compressed gas cylinder can be adjusted with the needle valve shown in Figure 35. The procedure that will be used to attempt to activate P3 will consist of discrete discharges of nitrogen, gradually increasing in volume, either until P3 is activated, or until the capacity of the nitrogen delivery system is reached.

PILOT-SCALE TEST RESULTS

At the time of the preparation of this Final Report, P3 had been evaluated in ambient temperature tests at the SRI laboratory, installed on the PSDF HGCU filter vessel tubesheet, and been exposed to about five days of HTHP conditions during the first phase of a PSDF gasification test run. Operational problems then caused this run to be temporarily halted. When this test run resumes, the manual activation of P3 with the injection of nitrogen can hopefully be attempted.

Figure 36 shows the results of one of the activation tests performed at ambient conditions at SRI's laboratory. These data show that P3 exhibits a much higher pressure drop (about 47 in. H_2O) than was measured for P2 (about 11 in. H_2O), presumably because of the alternate sealing approach used for P3. The flow rate required for activation at ambient conditions was about 88 acfm. When the increased gas density at the HTHP conditions in the PSDF is taken into account, P3 should require a gas flow of about 34 acfm to activate.

The pressure drop across P3 and the secondary failsafe above it have remained below 5 in. H_2O during the first phase of the ongoing PSDF test, indicating that P3 has remained in its inactive position.

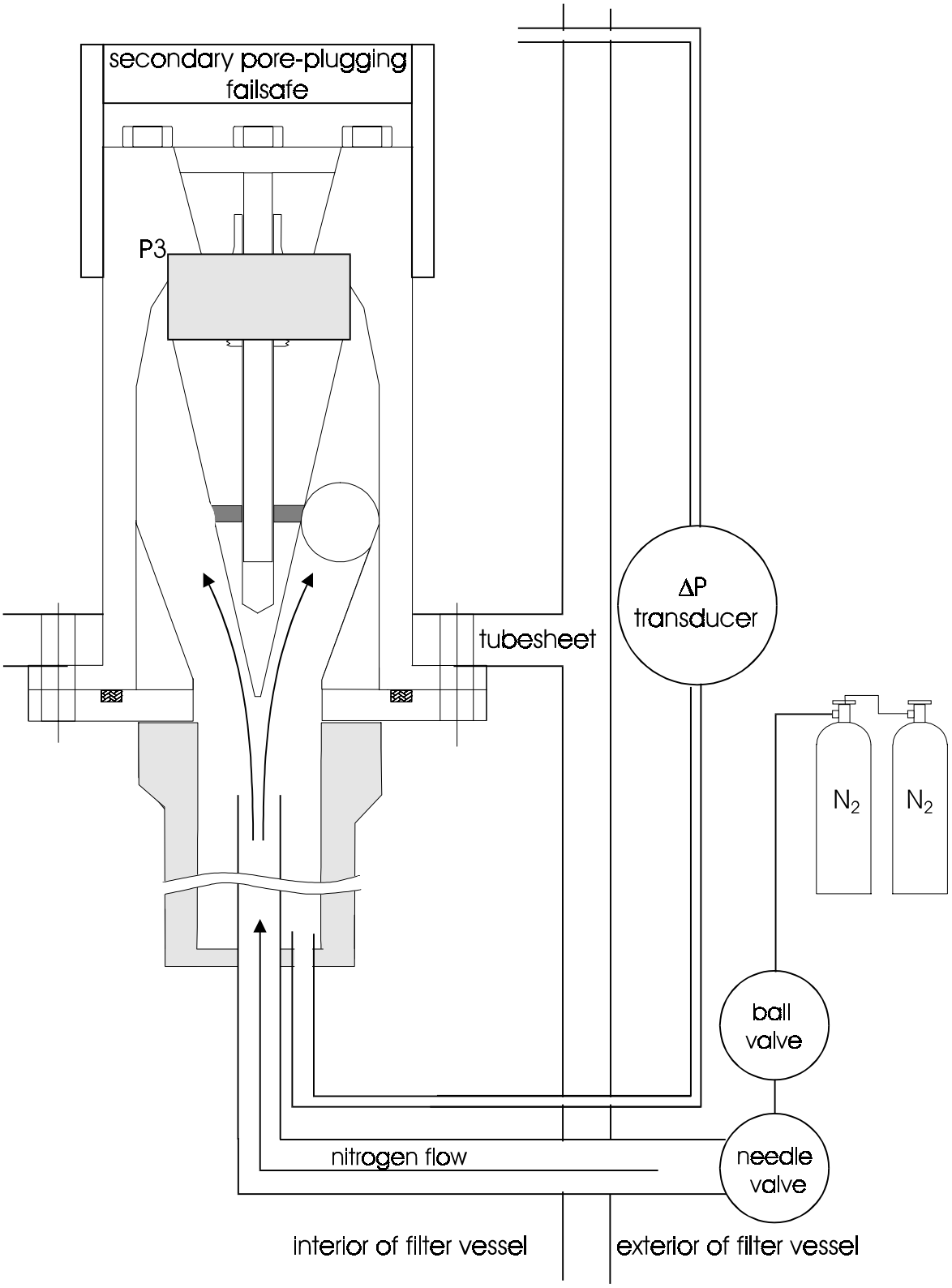

Figure 35. General arrangement of P3 in the PSDF filter vessel. (Details of the sealing design have been obscured.)

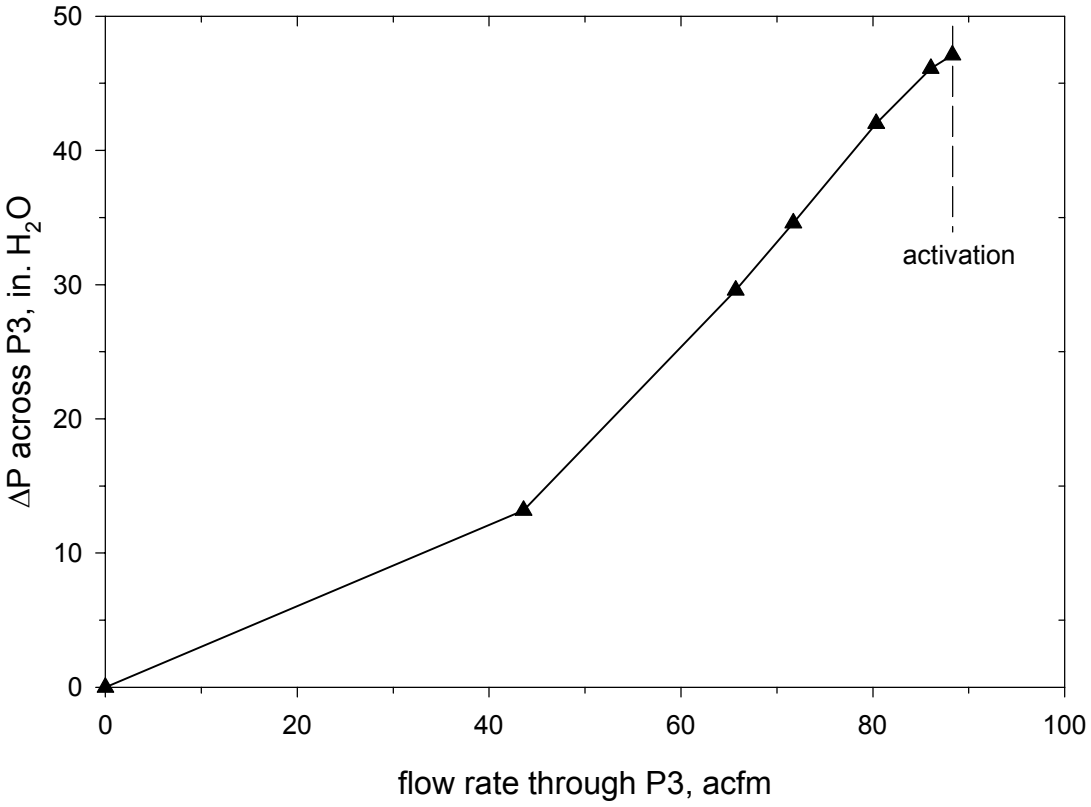

Figure 36. Pressure drop across P3 as a function of the flow rate through it.

CONCLUSIONS

The three prototype FFMSGDs (P1, P2, and P3) performed very well in the bench-scale tests and pilot-scale evaluations. Activations of these devices were repeatedly achieved at ambient and, for P2, HTHP conditions. (The activation of P3 at HTHP conditions will hopefully be accomplished in later testing at the PSDF.) The threshold of activation for the FFMSGD is properly quantified in terms of the quantity ρv^2, where ρ is the density of the gas passing through the SGD, and v is the velocity of the gas through the minimum annular orifice in the device. In all cases, the FFMSGDs activated quickly and completely. P1 proved the validity of the FFMSGD concept. Extensive HTHP tests were then performed with the first high-temperature prototype, P2. P2 remained activated (closed) when exposed to vigorous reverse-gas cleaning pulses. P2 also withstood these vigorous reverse-gas cleaning pulses in its inactive (open) mode with no apparent effect. The threshold of activation for P2 was consistent for almost all the test runs performed at both ambient and HTHP conditions. In one of the HTHP test runs performed with P2, the unexpected failure of the filter element under it resulted in the rapid activation of the FFMSGD. To the extent provided by the PCME device used to measure outlet mass levels at the DOE HTGSCTF, the activation of P2 quickly and consistently formed a high-quality seal. Post-test visual inspection of the seal formed by P2 when it activated at ambient and HTHP conditions suggests that the device formed a total barrier to the passage of particles, and also to the flow of gas.

In addition, P2 offered very little resistance to the flow of filtered gas (ΔP across P2 was less than 1.5 in. H_2O at a flow of 30 acfm). Although the test designed to assess the effect the presence of P2 on cleaning effectiveness had to be aborted due to filter element failure at the DOE test facility, there is every reason to believe that the low resistance to flow in the forward (normal) direction translates to an equally low interference with the effectiveness of reverse-gas cleaning pulses.

Although the HTHP tests of P3 at the PSDF are ongoing, the ambient temperature test results of P3 indicate that it activates at a consistent threshold. Data from the portion of the PSDF HTHP test run that is complete at this time have shown that P3 remained open (inactive) through the installation of the filter assembly, and also through about five days of HTHP test conditions. The planned HTHP activation trials for P3 at the PSDF, although they will be performed too late to be included in this Final Report, will complete the evaluation of the FFMSGD concept envisioned for this project.

RECOMMENDATIONS FOR ADDITIONAL TESTING

Because of the potential of the FFMSGD to serve as a check valve in a variety of extremely harsh process environments, it is important to investigate its abilities and limitations to the fullest extent possible. The completion of the ongoing pilot-scale test at the PSDF will generate important data on the performance of the FFMSGD. Beyond this test, the key to further evaluation and validation of the FFMSGD concept is to obtain even more exposure of the device to harsh process conditions, and to perform additional tests of activation at these process conditions. However, because HGCU filters are relatively rare, and their operating time is very limited, obtaining extended exposure to HTHP conditions will be a challenge. In addition, verifying the quality of the seal formed by a FFMSGD after activation is crucial, but also difficult, because monitors that can accurately sense and report particulate concentrations at or below 1 ppm in HTHP environments are only now being developed and validated.

COMMERCIALIZATION ISSUES

The ultimate value of the FFMSGD technology will be realized when pilot-scale and/or full-scale installations can be completely outfitted with FFMSGD units. Besides conducting the additional verifications of the technical validity of the FFMSGD concept as noted above, the ability of the device to be integrated into a variety of process designs, and the minimization of the manufacturing costs of the FFMSGD must also be considered.

INTEGRATION INTO EXISTING FILTER SYSTEMS

One of the primary strengths of the FFMSGD concept is that it can be fabricated entirely from materials suitable to the process environment. The major components of the FFMSGD are its shell and sealing plug, the locking balls, and the gasket (if needed) to join the two halves of the shell together. It is reasonable to expect that if the FFMSGD concept is being applied to a process stream, then the design of this process will have already identified appropriate machinable material(s) from which the various process components could be fabricated. With the exception of the gasket, and possibly the locking balls, any FFMSGD design should be able to be fabricated from this same process-proven material. (In most cases, the locking balls could also be produced from this same material, with the only limitation being production cost, which would diminish as the number of balls being produced increased.) The gasket that might need to be a part of the final FFMSGD design for a given process should also be able to be made from the same materials that other parts of the process require.

Because the basic design of the FFMSGD is a cylinder, and because the FFMSGD concept is adjustable in size and flow capacity, it should be straightforward to physically adapt its design to interface with a wide variety of process vessels and tubesheets. The designs of P2 and P3 were easily adapted to the tubesheets at the DOE HTGSCTF and the PSDF, respectively.

By applying the design nomograph as described above, the activation threshold and the safety margin to prevent unintended activation should be able to be reliably established during the FFMSGD design process. With respect to the ruggedness of the device, the trials performed with the prototypes have shown that the FFMSGD design can withstand the handling and vibration that might be expected at a typical process application.

MANUFACTURING ISSUES

The manufacturing processes required to commercialize the FFMSGD will differ significantly from the computer-controlled machining processes used to fabricate the three prototypes. Except for the locking balls, casting should be the preferred method for producing the basic components of FFMSGD units. It is expected that electron discharge machining techniques will be applied to refine the finishes of the sealing surfaces, the grooves down the sides of the lower shell, and possibly whatever mating surfaces are involved in locating the alignment pin. Depending on the type of activation seal used for the top of the sealing plug (lapped metal-to-metal spherical surfaces vs. the alternative seal design used for P3), it may or may not be necessary for the sealing surfaces on the plug and the upper shell to be lapped. The mating of the top and bottom halves of the shell will most likely be configured, possibly with flanges, gaskets, or perhaps welded joints, to adapt to the tubesheet and filter holding structures implemented by the HGCU filter system where the installation of the FFMSGD is planned.

With the help of the fabrication shop that produced the three prototype FFMSGD units that were evaluated in this project, it was possible to define a rough estimate of the per-unit cost for a manufacturing run of 3000 failsafe devices (the number of devices that would probably be needed for one 200 MW PFBC plant). The design that was used as the basis for this estimate is somewhat modified from the P2 prototype evaluated at DOE/NETL. The material for these units was assumed to be 310 SS. The primary steps in the manufacturing process would be the production of molds for casting each of the pieces of the device, casting of the pieces needed to construct the 3000 units, followed by machining of selected surfaces of these pieces. The final step would be lapping the spherical sealing surface of each shell with the sealing surface at the top of its sealing plug. This final step would result in matched sets of upper shells and sealing plugs. The cost estimate further assumes that machining will be required for a variety of critical surfaces. Depending primarily on the quality of the cast surfaces, some of the surfaces that are currently assumed to need machining following the casting process may ultimately not need to be machined. Each surface that is exempted from machining will decrease the final per-unit cost. Based on this approach, the per-unit cost for

a 3000-unit run is expected to be between $550 and $785. Because of the factors discussed above, this range should be considered as an upper cost limit for mass producing the basic device. This cost range is intended to be only a rough estimate, and should not be used as a quote for production. The cost for a version of the FFMSGD based on the P3 design should be somewhat less than $550 per unit.

DEVELOPMENT OF A CANDLE FILTER FAILURE SAFEGUARD DEVICE

FINAL REPORT

SRI-ENV-02-9875-F

Approved by

P. Vann Bush, Vice President
March 29, 2002